
The wave model

May 1995

By **Peter Janssen**

European Centre for Medium-Range Weather Forecasts

Abstract

In this set of lectures I would like to give a brief overview of the state-of-the-art of ocean wave modelling, ranging from a derivation of the evolution equation of the wave spectrum from the Navier–Stokes equations to the practice of wave forecasting. From validation studies using satellite data from Geosat and ERS-1 it appears that present-day wave models are reliable. In addition, it is known from experience that wave results depend in a sensitive manner on the quality of the driving surface winds. For these reasons ocean wave forecasting has certain benefits for atmospheric modelling. Two examples of these benefits are given. The program of these lectures is, therefore, as follows:

1. Derivation of the energy balance equation

1.1 Preliminaries—Dynamical equations, dispersion relation in deep and shallow-water, group velocity, energy density, Hamiltonian and Lagrangian for potential flow. The averaged Lagrangian.

1.2 Energy balance equation (adiabatic part)—The need for a statistical description of ocean waves: the wave spectrum.—From the averaged Lagrangian we show that the adiabatic rate of change of the wave spectrum is determined by advection (with the group velocity) and refraction.

1.3 Energy balance equation (physics)—From now on we only consider deep water. It is shown that, in addition to adiabatic effects, the rate of change of the wave spectrum is determined by: (a) energy transfer from wind; (b) non-linear wave-wave interactions; (c) dissipation by white capping.

2. The WAM model—The WAM model is the first model that solves the energy balance equation, including non-linear wave-wave interactions.

2.1 Energy balance for wind sea—Distinction between wind sea and swell. Empirical growth curves: fetch and duration limitation. Energy balance for wind sea according to the WAM model. Evolution of wave spectrum. Comparison with observations from JONSWAP.

2.2 Wave forecasting—Quality of wind field (SWADE). Validation of wind and wave analysis using ERS-1 altimeter data and buoy data.—Quality of wave forecast, forecast skill depends on whether sea state is dominated by wind sea or swell.

3. Benefits for atmospheric modelling

3.1 Use as a diagnostic tool—The apparent over-activity of the atmospheric model during the forecast is reflected in too high forecasted wave height. This is shown by comparing monthly mean wave forecasts with the verifying analysis.

3.2 Coupled wind-wave modelling—The energy transfer from atmosphere to ocean is sea state dependent. To be consistent one has to couple wind and waves to take the sea state dependent slowing down of the wind into account. Such a coupled wind-wave model gives an improved climate in the Northern Hemisphere. Also, the wind field in the tropics is affected, to a considerable extent, (e.g. in monsoon area and warm pool east of Indonesia).

Table of contents

1 . Derivation of the energy balance equation	1
1.1 Preliminaries	3
1.2 Energy balance equation (adiabatic part)	13
1.3 Energy balance equation (physics)	20
2 . The WAM model	33
2.1 Energy balance for wind sea	33
2.2 Wave forecasting	42

3 . Benefits for atmospheric modelling	51
3.1 Use as a diagnostic tool	51
3.2 Coupled wind-wave modelling	57
REFERENCES	60

1. DERIVATION OF THE ENERGY BALANCE EQUATION

In this chapter we shall try to derive the basic evolution equation of wave modelling, called the energy balance equation, from first principles. Our starting point is the Navier–Stokes equations for air and water and it is emphasised that there are two small parameters in the problem namely the steepness of the waves and the ratio of air to water density. Because of these two small parameters one may distinguish two scales in the time–space domain, namely a fast scale related to the period and wave length of the waves and a much longer time and length scale related to changes due to the small effects of non-linearity and growth of waves by wind.

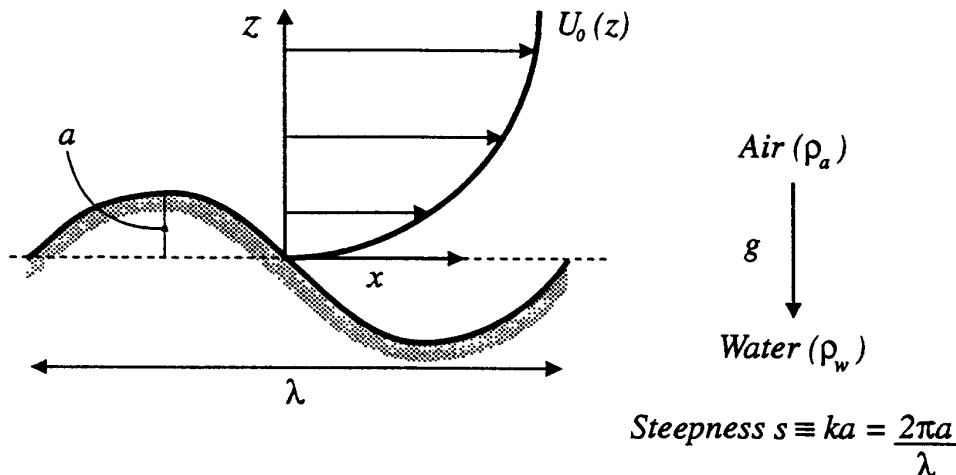


Figure 1. The problem

Using perturbation methods, an approximate evolution equation for the amplitude a and phase of the gravity waves may be obtained. In lowest-order one then deals with free surface gravity waves while higher-order terms represent the effects of wind input, non-linear (four) wave interaction and dissipation.

Applying this deterministic evolution equation to a practical application, such as ocean wave prediction, is not very feasible, however. First of all, we may have some information on the initial condition for the amplitude of the waves (but it should be stressed that this requires the 2-D wave spectrum), but certainly not on the phases of the waves. On the other hand, one might ask oneself whether all this detailed information regarding the phase of the waves is really needed. Perhaps we can content ourselves with knowledge about averaged quantities such as the wave spectrum $F(k)$, where

$$F(k) \sim a(k)a^*(k) \quad (1)$$

with a the complex amplitude of a wave with wave number k and a^* is the complex conjugate. A *statistical description* seems the most promising way to proceed.



Secondly, a standard approach would be to do a Fourier analysis of the deterministic evolution equations and solve the resulting ordinary differential equations on the computer. This approach is followed by ECMWF's atmospheric, spectral model. For water waves, this approach is not feasible because too many scales are involved. A typical ocean wave has length scales between 1 and 250 m, while a typical ocean basin extends over 10 000 km. A way of circumventing this problem is to employ a multiple-scale approach. We assume that there are two scales, one related to the free gravity waves and a long scale related to the aforementioned physical processes, such as wind input, non-linear interactions and dissipation. Since we know the solution for the free gravity waves, we only have to consider the evolution of the wave field on the long time and space scale, thus making the wave forecasting problem on a global scale a tractable problem. As a result, it turns out that the wave spectrum \mathcal{F} is a slowly varying function of space and time and its evolution equation, called the energy balance equation, will be derived in this chapter.

1.1 Preliminaries

Referring to Fig. 1 for the geometry, our starting point is the usual evolution equation for an incompressible, two-layer fluid, consisting of air and water. Introducing g for the acceleration of gravity and denoting the interface between air and water by $\eta(\mathbf{x}, t)$ we then have

$$\begin{aligned} \nabla \cdot \mathbf{u} &= 0 \\ \left(\frac{\partial}{\partial t} + \mathbf{u} \cdot \nabla \right) \mathbf{u} &= -\frac{1}{\rho} \nabla P - \mathbf{g} + \nabla \cdot \boldsymbol{\tau} \end{aligned} \quad (2)$$

with

$$\rho = \begin{cases} \rho_a, & z > \eta \\ \rho_w, & z < \eta \end{cases}$$

Velocities and forces (pressure and tangential stress) are continuous at the interface. A particle on either side of the surface will move in time Δt from $(\mathbf{x}, z = \eta(\mathbf{x}, t))$ to $(\mathbf{x} + \Delta \mathbf{x}, z + \Delta z = \eta(\mathbf{x} + \Delta \mathbf{x}, t + \Delta t))$ with $\Delta \mathbf{x} = \mathbf{u} \Delta t$ and $\Delta z = w \Delta t$. Thus, in the limit $\Delta t \rightarrow 0$ one obtains the kinematic boundary condition

$$\frac{\partial}{\partial t} \eta + \mathbf{u} \cdot \nabla \eta = w \quad (3)$$

Here, \mathbf{u} is the horizontal velocity at the interface while w is its vertical velocity. In order to complete the set of equations, one has to express the stress tensor $\boldsymbol{\tau}$ in terms of the mean flow. The stress contains the viscous stress and may or may not contain the additional stress resulting from turbulent fluctuation (the Reynolds stress).

For deep water, one has to specify boundary conditions at $z \rightarrow \pm\infty$: the oscillation should vanish in these limits. However, for water of finite depth the normal component of the velocity should vanish at the bottom.

In order to study the properties of pure gravity waves, we make the following approximations:

- (i) neglect viscosity and stresses. This gives the Euler equations. Continuity of the stress at the interface is no longer required. The parallel velocity at the interface may now be discontinuous.
- (ii) We disregard the air motion altogether because $\rho_a/\rho_w \ll 1$. In our discussion on wave growth we retain, of course, effects of finite air-water density ratio.

- (iii) We assume that the water velocity is irrotational. This is a reasonable approximation for water waves. In fact, it can be shown (homework!) that, in the framework of the Euler equations, the vorticity remains zero when it is zero initially.

We therefore introduce a velocity potential ϕ with the property

$$\mathbf{u} = \nabla\phi \quad (4)$$

and the flow is then described by Laplace's equation

$$\Delta\phi + \frac{\partial^2}{\partial z^2}\phi = 0, \quad \Delta = \frac{\partial^2}{\partial x^2} + \frac{\partial^2}{\partial y^2} \quad (5)$$

with two conditions at the surface

$$z = \eta \left\{ \begin{array}{l} \frac{\partial\eta}{\partial t} + \nabla\phi \cdot \nabla\eta = \frac{\partial}{\partial z}\phi \\ \frac{\partial\phi}{\partial t} + \frac{1}{2}(\nabla\phi)^2 + \frac{1}{2}\left(\frac{\partial\phi}{\partial z}\right)^2 + g\eta = 0 \quad (\text{Bernoulli}) \end{array} \right. \quad (6)$$

and a condition at $z = -D$ (a flat bottom is assumed here)

$$z = -D, \quad \frac{\partial}{\partial z}\phi = 0 \quad (7)$$

i.e. no fluid penetrates the bottom.

Eqs. (5)–(7) conserve the total energy of the fluid

$$E = \frac{1}{2}\rho g \int d\mathbf{x} \eta^2 + \frac{1}{2}\rho \int d\mathbf{x} \int_{-D}^{\eta} dz \left[(\nabla\phi)^2 + \left(\frac{\partial\phi}{\partial z}\right)^2 \right] \quad (8)$$

Here, the first term is the potential energy of the fluid while the second term is the kinetic energy.

By choosing appropriate canonical variables, [Zakharov](#) (1968), [Broer](#) (1974) and [Miles](#) (1977) independently found that E may be used as a Hamiltonian. The proper canonical variables are

$$\eta \quad \text{and} \quad \psi(\mathbf{x}, t) = \phi(\mathbf{x}, z = \eta, t) \quad (9)$$

The boundary conditions at the interface are then equivalent to Hamilton's equations

$$\frac{\partial\eta}{\partial t} = \frac{\delta E}{\delta\psi}, \quad \frac{\partial\psi}{\partial t} = -\frac{\delta E}{\delta\eta} \quad (10)$$

where $\delta E/\delta\psi$ is the functional derivative of E with respect to ψ .

Homework: Prove that (10) is equivalent to (6).

The formulation (10) has certain advantages. If one is able to solve the potential problem



$$\Delta\phi + \frac{\partial^2}{\partial z^2}\phi = 0$$

with boundary conditions

$$\phi(\mathbf{x}, z = \eta) = \psi \quad \text{and} \quad \frac{\partial}{\partial z}\phi(\mathbf{x}, z = -D) = 0$$

thereby expressing ϕ in terms of the canonical variables η and ψ , then the energy E can be evaluated in terms of η and ψ and the evolution of η and ψ follows at once from Hamilton's equations (10).

There is also a Lagrangian formulation of the water wave problem. Luke (1967) found that the variational principle

$$\delta \int dx dy dt \mathcal{L} = 0 \quad (11)$$

$$\text{with } \mathcal{L} = -\rho \int_{-D}^{\eta} dz \left[\frac{\partial}{\partial t}\phi + \frac{1}{2}(\nabla\phi)^2 + \left(\frac{\partial\phi}{\partial z}\right)^2 + gz \right],$$

gives the Laplace equation as well as the boundary conditions.

Intermezzo

Hamilton's equations are well-known from classical mechanics. Consider a particle with momentum p and position q in a potential well $V(q)$. The total energy of the particle is then given by

$$E = \frac{1}{2}\frac{p^2}{m} + V(q). \quad (12)$$

Regard p and q as canonical variables. Then, Hamilton's equations are ($\dot{q} = \partial q / \partial t$)

$$\dot{q} = \frac{\partial E}{\partial p} = \frac{p}{m} \quad (13a)$$

$$\dot{p} = -\frac{\partial E}{\partial q} = -\frac{\partial}{\partial q}V. \quad (13b)$$

Eliminating momentum p we get with $v = \dot{q}$

$$m\dot{v} = -\frac{\partial}{\partial q}V = \text{Force},$$

which we recognize as Newton's law where the Force is derived from the potential.

In classical mechanics, the Hamiltonian formulation follows from the principle of "least" action. To see this, consider the Lagrangian

$$\mathcal{L} = T - V = \frac{1}{2}m\dot{q}^2 - V(q) = \mathcal{L}(q, \dot{q}).$$

Newton's law then follows from the condition that the action be extremal, where

$$\text{action} = \int_{t_1}^{t_2} dt \mathcal{L}(q, \dot{q}) \quad (14)$$

The action is external if $\delta(\text{action}) = 0$ where

$$\begin{aligned} \delta(\text{action}) &= \int dt [\mathcal{L}(q + \delta q, \dot{q} + \delta \dot{q}) - \mathcal{L}(q, \dot{q})] \\ &= \int dt \left[\delta q \frac{\partial}{\partial q} \mathcal{L} + \delta \dot{q} \frac{\partial}{\partial \dot{q}} \mathcal{L} \right] \\ &= \int dt \left[\frac{\partial}{\partial q} \mathcal{L} - \frac{\partial}{\partial t} \frac{\partial}{\partial \dot{q}} \mathcal{L} \right] \delta q . \end{aligned}$$

As this should hold for arbitrary δq one finds that the action is extremal if q satisfies the Euler–Lagrange equations

$$\mathcal{L}_q - \frac{\partial}{\partial t} \mathcal{L}_{\dot{q}} = 0 \Leftrightarrow m\ddot{q} = -\frac{\partial}{\partial q} V \quad (15)$$

Defining the momentum p as

$$p = \mathcal{L}_{\dot{q}} \rightarrow \dot{q} = \dot{q}(p)$$

and regarding, from now on, p and q as independent variables, the Hamiltonian $H = H(p, q)$ is given by

$$H(p, q) = \dot{q} \mathcal{L}_{\dot{q}} - \mathcal{L} = \frac{1}{2} \frac{p^2}{m} + V(q) \quad (16)$$

Differentiating H with respect to q then gives, using (15)

$$\frac{\partial H}{\partial q} = -\mathcal{L}_q = -\frac{\partial}{\partial t} \mathcal{L}_{\dot{q}} = -\frac{\partial}{\partial t} p \rightarrow \frac{\partial p}{\partial t} = -\frac{\partial H}{\partial q}$$

which is just Eq. (13b), whereas differentiating H with respect to p gives

$$\frac{\partial H}{\partial p} = \frac{\partial \dot{q}}{\partial p} \mathcal{L}_{\dot{q}} + \dot{q} \frac{\partial}{\partial p} \mathcal{L}_{\dot{q}} - \mathcal{L}_{\dot{q}} \frac{\partial}{\partial p} \dot{q} = \dot{q}$$

which is just Eq. (13a).

All this is, however, less straightforward to do for a continuum such as the one we are dealing with. Nevertheless, Miles (1977) was able to derive from Luke's variational principle for water waves the Hamiltonian equations (10).

Homework:

Derive the governing equations for surface gravity waves (5)–(7) from Luke's variational principle. Hint: regard η and ϕ as the independent variables and consider $\delta \mathcal{L} = 0$.



Linear theory

We have now paid sufficient attention to the basics and it is now high time to derive the dispersion relation of surface gravity waves in the linear approximation. In linear theory, the evolution equations (5)–(7) for potential flow become

$$\Delta\phi + \frac{\partial^2}{\partial z^2}\phi = 0 \tag{17a}$$

with boundary conditions

$$z = 0, \quad \begin{cases} \frac{\partial\eta}{\partial t} = \frac{\partial\phi}{\partial z} \\ \frac{\partial\phi}{\partial t} + g\eta = 0 \end{cases} \tag{17b}$$

and

$$z = -D, \quad \frac{\partial\phi}{\partial z} = 0 \tag{17c}$$

In the case of water waves, the wave propagates horizontally so that the elementary sinusoidal solutions take the form

$$\eta = a \exp[i\theta], \quad \phi = Z(z) \exp[i\theta], \quad \theta = \mathbf{k} \cdot \mathbf{x} - \omega t.$$

From Laplace's equation this form of ϕ is a solution provided

$$Z'' - k^2 Z = 0, \quad k = |\mathbf{k}| = \sqrt{k_x^2 + k_y^2}.$$

For water of constant depth D the boundary condition on $z = -D$ requires $Z'(g) = 0$. Hence

$$Z \sim \cosh k(z + D).$$

Using the second equation of (17b) we thus find

$$\begin{aligned} \eta &= a \exp[i\theta] \\ \phi &= -\frac{ig}{\omega} a \frac{\cosh k(z + D)}{\cosh(kD)} \end{aligned} \tag{18}$$

However, we still have to satisfy the first equation of (17b). This imposes a restriction on the allowable frequency ω of the wave:

$$\boxed{\omega^2 = gk \tanh(kD)} \tag{19}$$

This is the dispersion relation of surface gravity waves.

We remark that the dispersion relation (19) tells us that there are, for given wave number k , two oscillations; name-

ly, waves propagating to the right and waves propagating to the left. In addition, it is important to distinguish between deep- and shallow-water waves.

Deep water (2D)

In deep water we have $D \rightarrow \infty$ and, therefore, (19) becomes

$$\omega^2 = gk.$$

The phase speed of the waves, $c = \omega/k$, is then given as

$$c = \sqrt{\frac{g}{k}} = \frac{g}{\omega}.$$

Therefore the high-frequency waves have the lowest phase speed. The energy of waves is advected by the group velocity $\partial\omega/\partial k$. For deep water waves the group velocity becomes

$$v_g = \frac{\partial\omega}{\partial k} = \frac{1}{2} \frac{g}{\omega}$$

hence, the group velocity is exactly half the phase speed. Furthermore, given the solution (18), it is straightforward to obtain the total energy of the waves. Using Eq. (8) we find for the energy density ε

$$\varepsilon = 2\rho g a a^*.$$

Shallow water

In shallow water the depth effects are really important, thus we take the limit of small depth and therefore (19) becomes

$$\omega^2 = k^2 gD \rightarrow \omega = \pm k \sqrt{gD}.$$

The most extreme example of shallow water waves are Tsunami's which are generated by earthquakes in the Gulf of Alaska. The resulting depression in the surface elevation has a large extent, thus the relevant wave length may be of the order to 500–1000 km. These waves are truly shallow water waves as the depth of the North Pacific is of the order to 5 km.

The phase speed of shallow water waves is given by

$$c = \frac{\omega}{k} = \sqrt{gD},$$

which is independent of wave number, hence there is no dispersion. As a consequence, the group velocity is equal to the phase speed,

$$v_g = \frac{\partial\omega}{\partial k} = c = \sqrt{gD}.$$

Note that in the above-mentioned example of Tsunami's the phase speed is of the order of 800 km/h!

Comparing deep and shallow water we note that there is an important difference between the two cases. Deep water



waves are highly dispersive, whereas really shallow water waves are not. Later we will see that this has important consequences for the non-linear evolution of surface waves. In fact, when waves are interacting with each other then, because of the dispersion, the interaction time will be finite. If there is no dispersion, however, the interaction time may become very long with the result that the effect of the non-linear interactions becomes very strong. We cannot deal with this in the weakly non-linear approach we are discussing here. We therefore consider only dispersive waves, so we will not discuss the extreme shallow water limit $kD \rightarrow 0$. Our results will therefore only be valid up to $kD = O(1)$.

Before we proceed we mention, without proof, that on a current \mathbf{U} that varies slowly in space and time, the angular frequency of the waves has a doppler shift. Hence, for waves on a current $\mathbf{U}(\mathbf{x}, t)$ we have

$$\omega = \mathbf{k} \cdot \mathbf{U} + \sigma, \tag{20}$$

where

$$\sigma = \pm \sqrt{gk \tanh(kD)}$$

This result also holds for slowly varying bottom profiles, i.e. $D = D(\mathbf{x}, t)$.

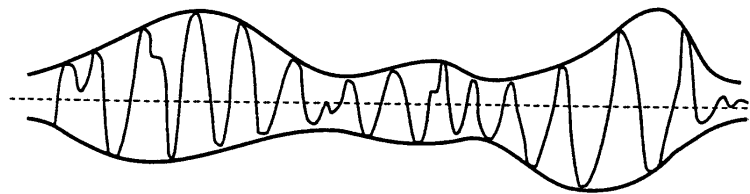


Figure 2. Waves come in groups.

Wave groups

In the previous section we have discussed a single wave. In practice we know, however, that waves come in groups (cf Fig. 2). Everyone who has done some sunbathing at the beach and has listened to the breaking waves knows that the seventh wave is the biggest. "Sting" even devoted a song to the subject (Love is the seventh Wave on the Dream of the blue Turtles).

If the wave groups are sufficiently long, we can give a reasonably accurate description by using a plane wave solution (cf Eq. (18)), however, with slowly varying phase and amplitude. Thus, similar to geometrical optics, wave groups may be described by,

$$\eta = a(\mathbf{x}, t) \exp[i\theta(\mathbf{x}, t)] + cc \tag{21}$$

where both amplitude a and phase θ are slowly varying functions of space and time. Here, slow has a relative meaning; it refers to the basic length (and time) scale imposed by the gravity wave, namely its wave length and period. Thus, we require

$$\frac{1}{a} \nabla a \ll k, \quad \frac{1}{a} \frac{\partial}{\partial t} a \ll \omega \quad \text{etc.}$$

Since the phase also is slowly varying, we may define a local angular frequency and wave number according to

$$\omega = -\frac{\partial}{\partial t}\theta, \quad \mathbf{k} = \nabla\theta \quad (22)$$

Assuming that the phase function θ is at least twice differentiable (e.g. $\partial^2\theta/\partial x\partial t = \partial^2\theta/\partial t\partial x$), Eq. (22) implies the following consistency relation, known as the equation of conservation of the number of wave crests:

$$\frac{\partial}{\partial t}\mathbf{k} + \nabla\omega = 0 \quad (23)$$

This equation tells us that, if the frequency of the wave depends on \mathbf{x} (because of slowly varying depth and or currents), the wave number will change in time. Eq. (23), therefore, provides a key element in the energy balance equation, namely refraction.

The evolution of amplitude a and frequency ω is not arbitrary either. To obtain these evolution equations one could, in principle, substitute the Ansatz (21), together with a similar Ansatz for the potential ϕ , into the basic equations (5)–(7). Then, by a straightforward but rather boring perturbation analysis the appropriate evolution equation for amplitude a and the dispersion relation for ω may be obtained.

We shall not follow this approach here. In its stead we prefer to give a derivation which starts from the Lagrangian (11). This approach, introduced by G B Whitham, is much more instructive. It gives a better insight into the underlying structure and it applies to any wave system that has a Lagrangian.

To that end, we simply substitute

$$\eta = a \exp[i\theta] + cc + \dots$$

into the Lagrangian density (11) and we average the Lagrangian over the rapidly varying phase θ .

Neglecting wave-induced currents, the average Lagrangian

$$\langle \mathcal{L} \rangle = \frac{1}{2\pi} \int d\theta \mathcal{L}$$

becomes (dropping the brackets)

$$\mathcal{L} = \frac{1}{2}\varepsilon \left\{ \frac{(\omega - \mathbf{k} \cdot \mathbf{U}_0)^2}{gkT} - 1 \right\} - \frac{1}{2} \frac{k^2 \varepsilon^2}{\rho g} \left\{ \frac{9T^4 - 10T^2 + 9}{8T^4} \right\} + O(\varepsilon^3) \quad (24)$$

where

$$\varepsilon = 2\rho g|a|^2, \quad T = \tanh(kD)$$

In other words, we obtain an average Lagrangian which depends on ω , \mathbf{k} and a

$$\mathcal{L} = \mathcal{L}(\omega, \mathbf{k}, a)$$

where $\omega = -\partial\theta/\partial t$ and $\mathbf{k} = \nabla\theta$. Hence, the appropriate evolution equations follow from the variational principle



$$\delta \int d\mathbf{x} dt \mathcal{L}(\omega, \mathbf{k}, a) = 0 \quad (25)$$

Variation with respect to the amplitude a then gives the dispersion relation

$$\frac{\partial}{\partial a} \mathcal{L} = 0 \quad (26a)$$

while variation with respect to the phase θ (note that θ appears in \mathcal{L} only through derivatives) gives the evolution equation for the amplitude

$$\frac{\partial}{\partial t} \mathcal{L}_\omega - \nabla \cdot \mathcal{L}_\mathbf{k} = 0 \quad (26b)$$

while a third equation follows from consistency (cf Eq. (23))

$$\frac{\partial}{\partial t} \mathbf{k} + \nabla \omega = 0. \quad (26c)$$

The set of equations describes the evolution of a slowly varying wave group. Note that (26a) is quite general as it is valid for any wave system that has a Lagrangian!

Before we now return to our problem of surface gravity waves, we finally introduce a transport velocity

$$\mathbf{u} = -\frac{\mathcal{L}_\mathbf{k}}{\mathcal{L}_\omega} \quad (27)$$

so that (26b) becomes

$$\frac{\partial}{\partial t} \mathcal{L}_\omega + \nabla \cdot (\mathbf{u} \mathcal{L}_\omega) = 0 \quad (28)$$

This equation describes the evolution of the action density \mathcal{L}_ω , a term which will become more plausible later.

Subsequently, we apply our results to the Lagrangian (24) in the linear approximation (i.e. disregard non-linear terms in ε). The Lagrangian (24) may then be written conveniently

$$\mathcal{L} = \frac{1}{2} \varepsilon D(\omega, \mathbf{k}) \quad (29)$$

where

$$D = \frac{(\omega - \mathbf{k} \cdot \mathbf{U}_0)^2}{gkT} - 1$$

The dispersion relation then immediately follows from Eq. (26a), or,

$$D = 0$$

hence, with $\sigma = \sqrt{gkT}$, we have

$$\omega = \mathbf{k} \cdot \mathbf{U}_0 \pm \sigma$$

which is to be compared with Eq. (20). Note that now the current \mathbf{U}_0 and depth D are allowed to be slowly varying functions of space and time. Finally, the equation for the action density

$$N = \mathcal{L}_\omega = \frac{\varepsilon}{\sigma} \quad (30)$$

becomes

$$\frac{\partial}{\partial t} N + \nabla \cdot \mathbf{v}_g N = 0 \quad (31)$$

where \mathbf{v}_g is the group velocity $\partial\omega/\partial\mathbf{k}$. Here, we remark that, for the (linear) group velocity, we have used the relation

$$\mathbf{v}_g = -\frac{D_{\mathbf{k}}}{D_\omega}$$

The importance of the action balance equation cannot be overemphasised. Eq. (31) has the form of a conservation law in which the local rate of change of a density is determined by a flux of that density. In fact, if one has zero flux at the boundaries of the ocean basin, one finds that the integral

$$N_{\text{tot}} = \int d\mathbf{x} N$$

is conserved. We emphasise that, in case of slowly varying bottom and currents, it is not the wave energy $E = \int d\mathbf{x} \varepsilon$ which is conserved, but it is the total action N_{tot} !

This conclusion may come as a surprise but it should be pointed out that it is a rather common feature in e.g. classical mechanics. Consider, for example, the well-know example of a pendulum in which the length is varied slowly. In that case E and frequency ω change when the length is varied but the 'adiabatic' invariant

$$A = \frac{E}{\omega}$$

is constant.

In closing, we stress once more that in slowly varying circumstances the wave energy is not conserved. However, the total energy of the system which includes contributions due to currents, e.g., is certainly conserved. If waves are considered in isolation (regarded as "the" system), then the energy is not conserved because of interactions with currents.

Homework "Adiabatic Invariants" Study this!

Consider once more a particle in a potential well and let us introduce an externally imposed change parametrized by some parameters $\lambda(t)$. The variational principle now becomes

$$\delta \int dt \mathcal{L}(q, \dot{q}, \lambda) = 0$$

and the variational equation is



$$\frac{d}{dt} \mathcal{L}_{\dot{q}} - \mathcal{L}_q = 0$$

We first calculate the average Lagrangian for period motion with λ fixed. If the period is $\tau = 2\pi/\nu$ (ν here is the frequency), then

$$\langle \mathcal{L} \rangle = \frac{\nu}{2\pi} \int_0^\tau \mathcal{L} dt$$

In periodic motion ($\lambda = \text{constant}$) we have conservation of energy $E = \dot{q} \mathcal{L}_{\dot{q}} - \mathcal{L}$ (check this). The relation may then be used to express \dot{q} as function of (q, E, λ) and then also the momentum $p = \mathcal{L}_{\dot{q}}$ can be expressed as

$$p = p(q, E, \lambda).$$

For (almost) periodic motion the average Lagrangian becomes

$$\langle \mathcal{L} \rangle = \frac{\nu}{2\pi} \oint p(q, E, \lambda) dq - E,$$

where \oint is a loop integrated over one complete period of oscillation.

We now allow slow variations of λ with consequent changes of ν and E and we use the average variation principle

$$\delta \int dt \mathcal{L}(\nu, E, \lambda) = 0.$$

Define again ν as the derivative $\dot{\theta}$ of a phase θ . Variation with respect to E and θ gives

$$\mathcal{L}_E = 0, \quad \frac{d}{dt} \mathcal{L}_\nu = 0$$

The first of these corresponds to the dispersion relation (26a) while the second corresponds to the action density equation (26b). Thus

$$\mathcal{L}_\nu = \frac{1}{2\pi} \oint p dq = \text{constant}$$

which is just the classical results of an adiabatic invariant. As the system is modulated, ν and E vary individually but

$$N(\nu, E) = \frac{1}{2\pi} \oint p dq$$

remains constant. The analogy between \mathcal{L}_ν of the oscillator and \mathcal{L}_ω of surface waves should be clear now.

1.2 Energy balance equation (adiabatic part)

In the previous section we have seen how free wave packets evolve on varying currents in basins with variable depth. The geometrical optics approach can, however, also be used in other situations. For example, one may study

the coupled problem which takes into account the effect of wind on waves. Or, one may consider nonlinear interactions or dissipation. As long as the perturbations are small they can be added and the action balance equation becomes

$$\frac{\partial}{\partial t} N + \nabla \cdot \mathbf{v}_g N = \left. \frac{\partial N}{\partial t} \right|_{\text{wind}} + \left. \frac{\partial N}{\partial t} \right|_{\text{nonlin}} + \left. \frac{\partial N}{\partial t} \right|_{\text{dissip}} \quad (32)$$

In the next section we shall give examples of how to derive the rate of change of the action density due to wind and due to nonlinear interactions. In this section we discuss in some detail the adiabatic part of the action balance equations.

Before we do this we have to introduce the concept of the wave spectrum. As already pointed out, solving the deterministic action balance (32) is not practical because knowledge of the phase of the waves is required as well. In order to avoid this problem we shall contend ourselves with a statistical description of the ocean surface.

We introduce, therefore, the homogeneous and stationary statistical theory of random waves. In such a theory, wave components are necessarily independent (random phases). As a consequence, the probability distribution of the ocean surface is approximately Gaussian. The (near) Gaussian property of the ocean surface follows in principle from the Central Limit Theorem which tells us that if the waves have random and independent phases then the probability distribution is Gaussian. The waves are approximately independent because they have propagated into a given area of the ocean from different distant regions. And, even if initially one starts with a highly correlated state then, because of the dispersion, waves become separated, thereby decreasing the correlation (in fact, for dispersive waves the loss of correlation is exponentially fast). In practice, therefore, one always finds that for dispersive ocean wave the Gaussian property holds.

We therefore contend ourselves with knowledge about average quantities such as the moments

$$\langle \eta(\mathbf{x}_1) \rangle, \langle \eta(\mathbf{x}_1)\eta(\mathbf{x}_2) \rangle, \text{ etc.}$$

where the brackets denote an ensemble average. In most practical situations it turns out that we then have sufficient information about the ocean surface. Since we assume that the mean of the surface elevation vanishes, we only have to consider the two-point correlation function

$$\langle \eta(\mathbf{x}_1)\eta(\mathbf{x}_2) \rangle.$$

In addition, we assume that the wave field is homogeneous (on the scale of the wave length, at least), i.e. the two-point correlation only depends on the distance $\mathbf{x}_1 - \mathbf{x}_2$. Introducing the distance $\mathbf{x}_1 - \mathbf{x}_2 = \boldsymbol{\xi}$ we, therefore, have to study the two-point correlation function,

$$R(\boldsymbol{\xi}) = \langle \eta(\mathbf{x} + \boldsymbol{\xi})\eta(\mathbf{x}) \rangle \quad (33)$$

The (frozen) wave-number spectrum is now defined as the Fourier transform of the correlation R .

$$F(\mathbf{k}) = \frac{1}{(2\pi)^2} \int d\boldsymbol{\xi} \exp[i(\mathbf{k} \cdot \boldsymbol{\xi})] R(\boldsymbol{\xi}) \quad (34)$$

Instead of considering a single wave, as we did in the previous section, we now take a continuum of waves. Realizing we have two modes (a positive frequency and a negative frequency mode) we write



$$\eta(\mathbf{x}, t) = \int_{-\infty}^{\infty} d\mathbf{k} \hat{\eta}_+(\mathbf{k}) \exp[i(\mathbf{k} \cdot \mathbf{x} - \omega_+ t)] + \int_{-\infty}^{\infty} d\mathbf{k} \hat{\eta}_-(\mathbf{k}) \exp[i(\mathbf{k} \cdot \mathbf{x} - \omega_- t)] \quad (35)$$

Since η is supposed to be real we have

$$\hat{\eta}_-(\mathbf{k}) = \hat{\eta}_+^*(-\mathbf{k})$$

and, therefore,

$$\eta(\mathbf{x}, t) = \int_{-\infty}^{\infty} d\mathbf{k} \hat{\eta}(\mathbf{k}) \exp[i(\mathbf{k} \cdot \mathbf{x} - \omega t)] + \text{c.c.} \quad (36)$$

where we have omitted the subscript + on $\hat{\eta}$, and where c.c. means complex conjugate. Substituting (36) into (33), and requiring a homogeneous two-point correlation function we must have

$$\begin{aligned} \langle \hat{\eta}(\mathbf{k}) \hat{\eta}(\mathbf{k}') \rangle &= 0 \\ \langle \hat{\eta}(\mathbf{k}) \hat{\eta}^*(\mathbf{k}') \rangle &= |\hat{\eta}(\mathbf{k})|^2 \delta(\mathbf{k} - \mathbf{k}') \end{aligned} \quad (37)$$

and the two-point correlation function becomes

$$R(\boldsymbol{\xi}) = \int d\mathbf{k} |\hat{\eta}(\mathbf{k})|^2 \exp[i\mathbf{k} \cdot \boldsymbol{\xi}] + \text{c.c.} \quad (38)$$

In view of (34) we, therefore, find that the wave-number spectrum is given as

$$F(\mathbf{k}) = 2|\hat{\eta}(\mathbf{k})|^2 \quad (39)$$

Setting $\boldsymbol{\xi}$ to zero in Eq. (38) and using (39) we have

$$\langle \eta^2 \rangle = R(0) = \int d\mathbf{k} F(\mathbf{k}) \quad (40)$$

then, as expected, the integral over the wave-number spectrum equals the wave variance $\langle \eta^2 \rangle$. Realising that, for propagating waves, potential and kinetic energy are equal, we find that the ensemble average of the wave energy $\langle E \rangle$ is related to the wave-number spectrum in the following manner

$$\langle E \rangle = \rho g \langle \eta^2 \rangle = \rho g \int d\mathbf{k} F(\mathbf{k}) \quad (41)$$

thus the wave-number spectrum indeed gives the distribution of wave energy over wave numbers.

Homework:

Check using linear wave theory that the ensemble average of E (of Eq. (8)) indeed satisfies relation (41).

We still face a problem of a somewhat technical nature. The spectrum introduced thus far is independent of space and time. Formally we have taken, namely, a Fourier transform over the whole domain. In order to allow for spatial dependence of the wave-number spectrum we simply adopt the procedure that we take the Fourier transform over a domain with such an extent that the two-point correlation function may still be regarded as homogeneous. On

the other hand, the domain should be large enough that it contains a sufficient number of waves. In practice, the extent of such a domain is of the order of 10–20 km.

We are now finally in the position to derive the action balance equation for a continuous spectrum. By analogy with the discrete case we can now introduce the action density spectrum $N(\mathbf{k})$ as

$$N(\mathbf{k}) = \frac{F(\mathbf{k})}{\sigma} \quad (42)$$

where, as before, $\sigma = \sqrt{gk \tanh kD}$. It is now tempting to use the action balance equation (32) for the discrete case to obtain the action balance equation for the continuous case. There is, however, one pitfall now. The evolution equation for $N(\mathbf{k})$ can only be a partial differential equation involving, for example, partial derivatives in time with position and wave number \mathbf{k} fixed. In other words, t , \mathbf{x} and \mathbf{k} are regarded as independent. In the discrete case the wave number is a local variable which depends on position and time.

The most convenient way to proceed is, therefore, to establish the following connection between the continuous action density spectrum and the discrete analog E/σ of Eq. (30). We are interested in the action density contained in modes with \mathbf{k} between $\mathbf{k} - (1/2)\Delta\mathbf{k}$ and $\mathbf{k} + (1/2)\Delta\mathbf{k}$. Introduce now a function $\varepsilon(\mathbf{k})$ with the definition

$$\varepsilon(\mathbf{k}) = \begin{cases} 1 & \text{if } -(1/2)\Delta\mathbf{k} < \mathbf{k} < (1/2)\Delta\mathbf{k} \\ 0 & \text{otherwise} \end{cases} \quad (43)$$

The appropriate connection between the discrete and continuous spectrum is

$$N(\mathbf{k})\Delta\mathbf{k} = \sum_{\mathbf{k}'} N_{\mathbf{k}'} \varepsilon(\mathbf{k} - \mathbf{k}'), \quad N_{\mathbf{k}'} = \frac{2|\alpha_{\mathbf{k}'}|^2}{\sigma} \quad (44)$$

So the sum is over all the modes with wave numbers contained in the above mentioned interval. We emphasise that the 'local' wave number \mathbf{k}' may depend on space \mathbf{x} and time.

The evolution equation for $N(\mathbf{k})$ is now readily obtained by starting to evaluate

$$\left. \frac{\partial N(\mathbf{k})}{\partial t} \right|_{\mathbf{x}, \mathbf{k}}$$

using (44) and the action balance equation (32). The result is

$$\frac{\partial}{\partial t} N + \nabla_{\mathbf{x}} \cdot (\mathbf{v}_g N) - \nabla_{\mathbf{k}} \cdot (\nabla_{\mathbf{x}} \Omega N) = S = S_{\text{wind}} + S_{\text{nonlin}} + S_{\text{dissip}} \quad (45)$$

Here, the term involving the partial derivative with respect to \mathbf{k} stems from the spatial and temporal dependence of the local wave number in the discrete case. It gives rise to the so-called refraction of the waves. Furthermore, Ω denotes just the usual dispersion relation

$$\Omega = \mathbf{k} \cdot \mathbf{U} + \sigma, \quad \sigma = \sqrt{gk \tanh kD} \quad (46)$$

and the group velocity $\mathbf{v}_g = \partial\Omega/\partial\mathbf{k}$. Finally, the source term, S is just the ensemble mean of the right-hand side of the Eq. (32). We shall discuss these terms in more detail in the next section.



We close this section by discussing some properties of the action balance equation in the absence of sources and sinks (adiabatic effects therefore).

Before we start this discussion we present a slightly more general form of the action balance equation. Let x_1 and x_2 be the spatial coordinates and k_1, k_2 the wave coordinates and let

$$\mathbf{z} = (x_1, x_2, k_1, k_2) \quad (47)$$

be their combined four-dimensional vector. Then the most fundamental form of the transport equation for the action density spectrum $N(\mathbf{k}, \mathbf{x}, t)$, without the source term, can be written in the flux form

$$\frac{\partial}{\partial t} N + \frac{\partial}{\partial z_i} (z_i N) = 0 \quad (48)$$

where z denotes the propagation velocity of a wave groups in the four-dimensional phase space of \mathbf{x} and \mathbf{k} . This equation holds for any rectangular coordinate system and for any field z , hence also for velocity fields which are not divergence free in four-dimensional phase space. In the special case when \mathbf{x} and \mathbf{k} represent a canonical vector pair—this is the case, for example, when they are the usual vector pairs—the propagation equations for a wave group (also known as Hamilton's equations of motion) read:

$$\begin{aligned} \dot{x}_i &= + \frac{\partial}{\partial k_i} \Omega \\ \dot{k}_i &= - \frac{\partial}{\partial x_i} \Omega \end{aligned} \quad (49)$$

where Ω denotes the dispersion relation (46).

The Hamilton equations have some intriguing consequences. Firstly, the transport equation for the action density may be expressed in the advection form

$$\frac{\partial}{\partial t} N = \frac{\partial N}{\partial t} + z_i \frac{\partial}{\partial z_i} N = 0 \quad (50)$$

as, because of (49), the field z , for a continuous ensemble of wave groups is divergence free in four-dimensional phase space,

$$\frac{\partial}{\partial z_i} z_i = 0 \quad (51)$$

Thus, along a path in four-dimensional phase space defined by the Hamilton equations (49) the action density is conserved. This property holds only for canonical coordinates for which the flow divergence vanishes [the so-called Liouville Theorem].

Secondly, the analogy between Hamilton's formalism of particles with a Hamiltonian H and wave groups obeying the Hamilton equations of motion should be pointed out. Indeed, wave groups may be regarded as particles and the Hamiltonian H and angular frequency Ω play similar roles. Because of this similarity Ω is expected to be conserved as well (under the restriction that Ω does not depend on time). This can be verified by direct calculation of the rate of change of Ω following the path of a wave group in phase space,

$$\frac{d}{dt}\Omega = z_i \frac{\partial}{\partial z_i}\Omega = x_i \frac{\partial}{\partial x_i}\Omega + k_i \frac{\partial}{\partial k_i}\Omega = 0 \quad (52)$$

The vanishing of $d\Omega/dt$ follows at once upon using the Hamilton equations (49). Note that the restriction of no time dependence of Ω is essential for the validity of (52), just as the Hamiltonian H is only conserved when it does not depend on time t . Thus, (52) gives the important message that angular frequency is conserved when following a wave group.

We now turn to the important case of spherical coordinates. Since (48) holds for any rectangular coordinate system, the transport equation in spherical geometry is easily obtained. To that end let us consider the spectral action density $\hat{N}(\omega, \theta, \phi, \lambda, t)$ with respect to angular frequency ω and direction θ (measured clockwise relative to true north) as a function of latitude ϕ and longitude λ . The reason for the choice of frequency as the independent variable (instead of, for example, the wave number k) is that, for a fixed topography and current, the frequency Ω is conserved when following a wave group, therefore the transport equation simplifies. In general, the conservation equation for \hat{N} thus reads

$$\frac{d}{dt}\hat{N} + \frac{\partial}{\partial\phi}(\dot{\phi}\hat{N}) + \frac{\partial}{\partial\lambda}(\dot{\lambda}\hat{N}) + \frac{\partial}{\partial\omega}(\dot{\omega}\hat{N}) + \frac{\partial}{\partial\theta}(\dot{\theta}\hat{N}) = 0 \quad (53)$$

and, since $\dot{\omega} = \partial\Omega/\partial t$, the term involving the derivative with respect to ω drops out in case of time-independent current and bottom. The action density \hat{N} is related to the normal spectral density N with respect to a local cartesian frame (x, y) through $\hat{N} d\omega d\theta d\phi d\lambda = N d\omega d\theta dx dy$, or

$$\hat{N} = NR^2 \cos\phi \quad (54)$$

where R is the radius of the earth. Substitution of (54) into (53) yields the transport equation

$$\frac{\partial}{\partial t}N + (\cos\phi)^{-1} \frac{\partial}{\partial\phi}(\dot{\phi} \cos\phi N) + \frac{\partial}{\partial\lambda}(\dot{\lambda}N) + \frac{\partial}{\partial\omega}(\dot{\omega}N) + \frac{\partial}{\partial\theta}(\dot{\theta}N) = 0 \quad (55)$$

where, with v_g the magnitude of the group velocity,

$$\begin{aligned} \dot{\phi} &= (v_g \cos\theta - U_0)/R \\ \dot{\lambda} &= (v_g \sin\theta - V_0)/(R \cos\phi) \\ \dot{\theta} &= v_g \sin\theta \tan\phi/R + (\mathbf{k} \times \mathbf{k})/k^2 \\ \dot{\omega} &= \partial\Omega/\partial t \end{aligned} \quad (56)$$

represents the rates of change of the position and propagation direction of a wave packet. Here, U_0 and V_0 are the components of the current in northerly and easterly direction respectively. Eq. (55) is the basic transport equation which will be used in the numerical wave-prediction model.

We finally mention the following properties:

- (a) *Great circle propagation on the globe.* A wave group propagates along a great circle over the globe. The proof of this can be given but is rather tedious (cf Komen et al, 1994, pp. 210–211). This property is related to the presence of refraction on the globe, even in the absence of depth and current refraction ($\mathbf{k} = 0$). From (56) we see that there is then a rate of change of direction according to



$$\dot{\theta} = v_g \sin \theta \tan \phi / R \quad (57)$$

This refraction is entirely due to the change in time of the local northward pointing vector and is, therefore, apparent because it is related only to the choice of coordinate system.

- (b) *Shoaling.* Consider now finite depth effects in the absence of currents. Shoaling of waves already occurs for wave propagation parallel to the direction of the depth gradient. In this case we ignore depth refraction, because $\dot{\mathbf{k}} \times \mathbf{k} = 0$. In addition, we take the wave direction θ to be zero (northerly propagation) so that the longitude is constant ($\dot{\lambda} = 0$) and $\dot{\theta} = 0$. In the steady state, the transport equation becomes

$$\frac{1}{\cos \phi} \frac{\partial}{\partial \phi} (\dot{\phi} \cos \phi N) = 0 \quad (58)$$

where in this special case $\dot{\phi} = v_g / R$ and the group speed only depends on latitude (since the depth profile depends on ϕ). Hence, we immediately find conservation of the action density flux in the latitude direction, or,

$$\frac{v_g \cos \phi}{R} N = \text{constant}$$

Now, if the depth decreases for increasing latitude, conservation of flux requires an increase of action density as the group speed decreases for decreasing depth. This phenomenon, which occurs in coastal areas, is called shoaling. Its most dramatic consequences may be seen when tidal waves, generated by earthquakes, approach the coast resulting in tsunamis.

- (c) *Refraction.* We again assume no current and no time dependence. As a general principle one can then state that wave rays (the path of the wave group in \mathbf{x} -space) will bend towards shallower water resulting in, for example, focusing phenomena and caustics. In this way a sea mountain plays a similar role for gravity waves as a lens for light waves. Furthermore, because of this general principle, close to the coast waves will always propagate towards the coast, even if far away from the coast they propagate parallel to it. All these examples of this general principle may be explained in terms of refraction. The refraction is given by the rate of change of the wave direction, $\dot{\theta}$. Writing (56) in more explicit form we have

$$\dot{\theta} = \frac{\sin \theta \frac{\partial}{\partial \phi} \Omega - \frac{\cos \theta}{\cos \phi} \frac{\partial}{\partial \lambda} \Omega}{kR} \quad (59)$$

Consider then again as an example waves propagating north ($\theta = 0$) parallel to the coast. Suppose now that depth depends only on longitude such that it decreases towards the shore. Thus

$$\dot{\theta} = -\frac{1}{kR \cos \phi} \frac{\partial}{\partial \lambda} \Omega > 0$$

since $\partial \Omega / \partial \lambda < 0$ (depth decreases), hence the wave ray will bend towards the coast.

- (d) *Current effects.* Currents may give rise to effects similar to (depth) refraction. However, the most dramatic effects may be found when the waves propagate against the current. For sufficiently large

current, wave propagation is prohibited and wave reflection occurs. The most prominent example of this is found in the Agulhas current, east of South Africa. A more detailed explanation of this effect is given in [Komen et al. \(1994\)](#), p. 214. Here, we just point out that it really follows from the dispersion relation which, for a simple 1-D case in case of propagation against a current reads

$$\Omega = \sqrt{gk} - kU_0$$

where we took the deep water limit. Then, the group velocity $\partial\Omega/\partial k$ vanishes for $k = g/(4U_0^2)$ and wave propagation is not possible any more.

1.3 Energy balance equation (physics)

In this section we shall discuss some of the physical effects that are relevant for wave evolution. Only deep water waves are considered here, although shallow water effects can be incorporated rather straightforwardly.

The physical processes we shall study are the generation of waves by wind and wave-wave interactions. The source term for dissipation is less easy to study so we will only give its form at the end of this section.

Wind input and non-linear interactions have one important feature in common, namely they are both examples of a resonant interaction. Consider generation of waves by wind. We have seen that in lowest order we are dealing with pure surface gravity waves. These waves have a certain phase speed $c(k)$. Above the waves we have a certain non-uniform airflow $U(z)$ and at the height z_c where $U(z_c) = c(k)$ the airflow always sees the same phase of the wave. The height z_c is called the critical height and the air around that height may enjoy a resonant interaction with the gravity wave. This example of wave mean flow interaction was given by [Miles \(1957\)](#). The result is exponential growth of the gravity wave and therefore this mechanism is called Miles' instability. Non-linear interactions are another example of resonant interaction. Again we start from the pure gravity waves and we realize that non-linear terms may give contributions of the following type

$$\exp[i(\theta_2 + \theta_3)] , \quad \exp[i(\theta_2 + \theta_3 + \theta_4)] , \quad \text{etc.}$$

Now, if the sum of those phases θ_i matches the phase of one of the linear waves (call this phase θ_1), or

$$\theta_1 = \theta_2 + \theta_3 , \quad \theta_1 = \theta_2 + \theta_3 + \theta_4 , \quad \text{etc.}$$

then the non-linear terms may drive the linear waves resonantly, giving rise to an energy transfer between wave 1 and waves 2, 3, etc. The resonance conditions on the phases boil down to the following resonance conditions for wave number \mathbf{k} and angular frequency ω

$$\omega_1 = \omega_2 + \omega_3 , \quad \mathbf{k}_1 = \mathbf{k}_2 + \mathbf{k}_3 , \quad [3\text{-wave interaction}]$$

$$\omega_1 = \omega_2 + \omega_3 + \omega_4 , \quad \mathbf{k}_1 = \mathbf{k}_2 + \mathbf{k}_3 + \mathbf{k}_4 , \quad [4\text{-wave interaction}]$$

and [Phillips \(1958\)](#) discovered that for gravity waves, three-wave interactions are not possible. However, four-wave interactions do exist. [Hasselmann \(1962\)](#) then subsequently derived the rate of change of the action density for an ensemble of gravity waves.

It should be realised that the descriptions of the physical processes we are going to present now are an idealisation of reality. Both in water and air we have, in reality, turbulent fluctuations which might upset the delicate resonant interactions. Nevertheless, these simplified models of reality give realistic results.

Energy transfer from wind

The problem of wind-wave generation is closely related to the instability of a plane parallel shear flow. We therefore study the stability of the equilibrium solution (see Fig. 3)

$$\begin{aligned} \mathbf{U}_0 &= U_0(z)\hat{e}_x, \quad \mathbf{g} = -g\hat{e}_z \\ \rho_0 &= \rho_0(z), \quad P_0(z) = g\int dz \rho_0(z) \end{aligned} \tag{60}$$

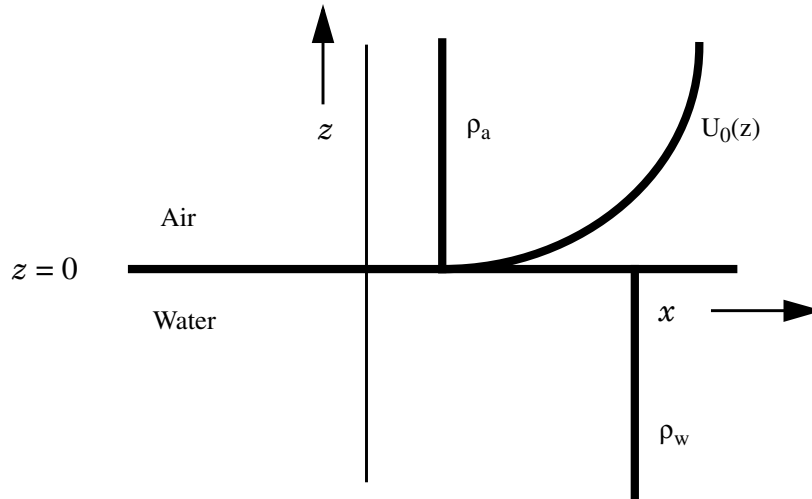


Figure 3. Equilibrium profiles of density and velocity.

Our starting point is slightly more general than equation (2). We take an adiabatic fluid with "infinite" sound speed. Hence,

$$\begin{aligned} \nabla \cdot \mathbf{u} &= 0 \\ \frac{d}{dt}\mathbf{u} &= -\frac{1}{\rho}\nabla p + \mathbf{g} \\ \frac{d}{dt}\rho &= 0 \end{aligned} \tag{61}$$

We shall only consider propagation in one direction (the x -direction). Using Squire's theorem (Drazin and Reid, 1981) results may be generalised to the 2-dimensional case. Linearisation and taking normal modes of the form $\rho_1 \sim \exp i\theta$, $\theta = kx - \omega t$, one obtains

$$\begin{aligned} ik u + \partial w / \partial z &= 0 \\ ik W u + w W' &= -ik p_1 / \rho_0 \\ ik W w &= \rho_1 p_0' / \rho_0^2 - (\partial p_1 / \partial z) / \rho_0 \\ ik W \rho_1 + w \rho_0' &= 0 \end{aligned} \tag{62}$$

where $\mathbf{u}_1 = (u, 0, w)$, $W = U_0 - c$, $c = \omega/k$ and the prime denotes differentiation of an equilibrium quantity with respect to height z . After some algebra one then arrives at the following Sturm–Liouville differential equation for the displacement $\psi \sim w/W$ of the streamlines

$$\frac{d}{dz} \left(\rho_0 W^2 \frac{d}{dz} \psi \right) - \psi (k^2 \rho_0 W^2 + g \rho_0') = 0 \quad (63)$$

which is subject to the boundary condition of vanishing displacement at infinite height or depth,

$$\psi \rightarrow 0, \quad |z| \rightarrow \infty \quad (64)$$

The boundary value problem (63)–(64) determines, in principle, the real and imaginary parts of the complex phase speed $c = \omega/k$ giving the growth rate $\gamma_a = \text{Im}(\omega)$ of the waves. The next step is now to specify in more detail the density profile $\rho_0(z)$ and the velocity $U_0(z)$.

In water we assume no current and a constant density. The eigenvalue problem then simplifies considerably. We have (for $z > 0$)

$$\frac{d^2}{dz^2} \psi_w = k^2 \psi_w \quad (65)$$

which gives, using the boundary condition at minus infinity, the solution

$$\psi_w = A \exp[kz] \quad (66)$$

The boundary condition at the interface between air and water is derived from an integration of Eq. (63) from -0 to $+0$. Note that at $z = 0$ the density profile shows a jump so that near $z = 0$, $\rho_0' = (\rho_a - \rho_w) \delta(z)$, where $\delta(z)$ is the Dirac delta-function. Requiring now that the displacement ψ of the streamline be continuous across the interface, we obtain from (63)

$$\rho_0 W^2 \frac{d}{dz} \psi \Big|_{-0}^{+0} = \int_{-0}^{+0} dz \psi [\rho_0 k^2 W^2 + g \rho_0'] \quad (67)$$

Since in the limit only the integral involving ρ_0' gives a contribution we obtain, using (66), the following dispersion relation for the phase speed of the waves:

$$c^2 = \frac{g(1-\varepsilon)}{k - \varepsilon \psi_a'(0)}, \quad \varepsilon = \frac{\rho_a}{\rho_w} \quad (68)$$

where, without loss of generality, we have taken the amplitude $A = 1$ as we deal with a linear problem. In air we take a constant density so that the eigenvalue problem (63)–(64) simplifies to

$$\begin{cases} \frac{d}{dz} W^2 \frac{d}{dz} \psi_a = k^2 W^2 \psi_a, & z > 0 \\ \psi_a(0) = 1, & c^2 = g(1-\varepsilon)/(k - \varepsilon \psi_a'(0)) \\ z \rightarrow \infty, & \psi_a \rightarrow 0 \end{cases} \quad (69)$$

Note that the air–water density ratio only occurs in the dispersion relation. In the absence of air ($\varepsilon \rightarrow 0$) we obtain the usual dispersion relation for deep water gravity waves. The effect of air on the surface waves is small as $\varepsilon \approx 10^{-3}$. We, therefore, solve the dispersion relation in an approximate manner with the result



$$c = c_0 + \varepsilon c_1 + \dots \quad (70)$$

where $c_0 = \sqrt{gk}$ and $c_1 = (1/2)c_0(\psi_a'/k - 1)$. As a result, the problem (69) now reduces to

$$\begin{cases} \frac{d}{dz} W_0^2 \frac{d}{dz} \psi_a = k^2 W_0^2 \psi_a, & z > 0 \\ \psi_a(0) = 1 \\ z \rightarrow \infty, & \psi_a \rightarrow 0 \end{cases} \quad (71)$$

where $W_0 = U_0 - c_0$ is now known. As c_0 is known already, the solution of the differential equation is simplified considerably. In addition, we now have an explicit expression for the growth rate γ_a of the waves,

$$\frac{\gamma_a}{\omega_0} = \varepsilon \text{Im} \left(\frac{c_1}{c_0} \right) = \frac{\varepsilon}{2k} \text{Im}(\psi_a') = \frac{\varepsilon}{4k} \mathcal{W}(\psi_a, \psi_a^*) \Big|_{z=0} \quad (72)$$

where the Wronskian \mathcal{W} is given as

$$\mathcal{W}(\psi_a, \psi_a^*) = -i(\psi_a' \psi_a^* - \psi_a \psi_a'^*) \quad (73)$$

Finally, before we give some interpretation of the result (72), we remark that it is rather common to use the vertical component of the wave-induced velocity instead of the displacement of the streamline $\psi \sim w/W$. The eigenvalue problem (71) then becomes, in terms of the normalised vertical velocity $\chi = w/w(0)$,

$$\begin{cases} W_0 \left(\frac{d^2}{dz^2} - k^2 \right) \chi = W_0'' \chi \\ \chi(0) = 1 \\ z \rightarrow \infty, & \chi \rightarrow 0 \end{cases} \quad (74)$$

and the growth rate of the waves is given by

$$\frac{\gamma_a}{\varepsilon \omega_0} = \frac{1}{4k} \mathcal{W}(\chi, \chi^*) \Big|_{z=0} \quad (75)$$

where the Wronskian \mathcal{W} is now given by $\mathcal{W} = -i(\chi' \chi^* - \chi \chi'^*)$.

Regarding Eq. (74) we remark that the differential equation (known as Rayleigh's equation) has a singularity at $W_0 = U_0 - c_0$. Since $W_0 = 0$ defines the critical height z_c (i.e. the height where the phase speed of the wave matches the wind speed) it is now clear that the resonance at the critical height z_c plays a special role in the problem of wind-wave generation.

Furthermore, we remark that the Wronskian \mathcal{W} is related to a physical quantity, known as the wave induced stress $\tau_w \equiv -\langle u_1 w_1 \rangle$. The result (75) is a very elegant one as it relates the growth of the waves to the wave-induced stress. In order to see this we recall that we are dealing with normal modes of the type $u_1 = u \exp[i\theta] + \text{c.c.}$, so that

$$\tau_w = -\langle (u \exp[i\theta] + \text{c.c.})(w \exp[i\theta] + \text{c.c.}) \rangle = -\{u w^* + \text{c.c.}\}$$

Using $\nabla \cdot \mathbf{u} = 0$ to eliminate u we thus have

$$\tau_w = -\frac{i}{k}[w^* w' - w w'^*]$$

and this indeed corresponds to the Wronskian \mathcal{W} of Eq. (75).

The Wronskian \mathcal{W} plays a special role in the theory of second-order differential equations. (This is therefore another reason why the result (75) is so elegant). Namely, by means of the Rayleigh equations (74) it may be shown that the Wronskian \mathcal{W} is independent of height except at the critical height, where it may show a jump (cf Fig. 4 for wave-induced stress).

We can check this by calculating the derivative of \mathcal{W} with respect to z and using Rayleigh's equation:

$$\frac{d}{dz} \mathcal{W} = -i(\chi^* \chi'' - \chi \chi''^*)$$

Using Rayleigh this becomes

$$\frac{d}{dz} \mathcal{W} = -i\left(k^2 |\chi|^2 + \frac{W_0''}{W_0} |\chi|^2 - \text{c.c.}\right) \quad (76)$$

Now for $z \neq z_c$ ($W_0 \neq 0$) we immediately find that \mathcal{W} , and hence the wave-induced stress, is independent of height. Since the wave-induced velocity vanishes for large height, we conclude that for $z > z_c$, \mathcal{W} vanishes, but may have a finite value for $z < z_c$. In fact, the jump at $z = z_c$ may be obtained from (76) by a proper treatment of the singularity at the critical height.

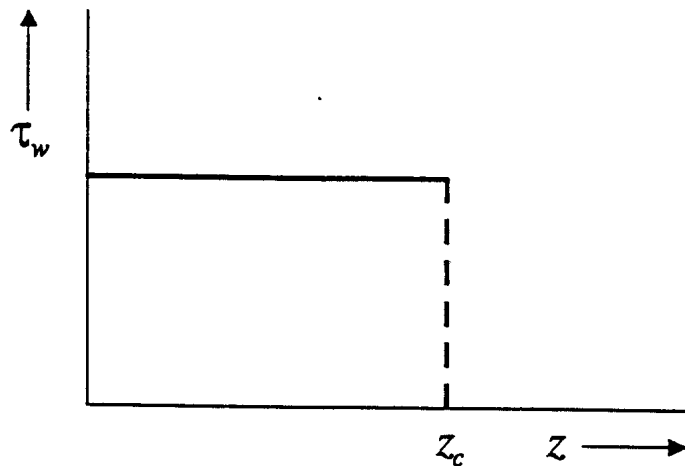


Figure 4. Wave-induced stress shows a jump at critical height.

To that end we consider the singular function

$$\frac{1}{W_0} \rightarrow \frac{1}{W_0 - i\delta}$$

and we take the limit for positive vanishing δ . Then,



$$\frac{1}{W_0} \rightarrow \frac{P}{W_0} + \pi i \delta(W_0)$$

and (76) becomes

$$\frac{d}{dz} \mathcal{W} = 2\pi W_{0c}'' |\chi_c|^2 \delta(W_0) \quad (77)$$

where the subscript c refers to evaluation at the critical height $z_c (W_0 = 0)$.

Integration of (77), using the boundary condition that \mathcal{W} vanishes for $z > z_c$, gives

$$z < z_c, \quad \mathcal{W} = -2\pi \frac{W_{0c}''}{|W_{0c}'|} |\chi_c|^2 \quad (78)$$

and therefore the growth rate of the waves (75) becomes

$$\frac{\gamma_a}{\epsilon \omega} = -\frac{\pi}{2k} \frac{W_{0c}''}{|W_{0c}'|} |\chi_c|^2. \quad (79)$$

This is Miles' classical result for the growth of surface gravity waves due to the shear flow. From Eq. (79) we obtain the well-known result that only those waves are unstable for which the curvature U_0'' of the wind profile at the critical height is negative. This is, for example, the case for a logarithmic wind profile.

There is, however, an important consequence of the instability of surface waves. While the waves are growing and, therefore, receiving energy and momentum from the air flow, a slowing down of the air flow by the gravity wave will result. The waves therefore give rise to a force which is the gradient of the wave-induced stress τ_w . Since the wave-induced stress is proportional to the Wronskian \mathcal{W} , which has a step function discontinuity at the critical height, the force is a delta-function. This suggests an important limitation of linear theory because a considerable wave/mean-flow interaction may therefore occur, giving rise to a modified mean flow. We discuss more details of the wave-mean-flow interaction in a short while, after we have compared results of the linear theory with observation.

In order to solve the boundary wave problem (74), we finally have to specify the shape of the wind profile. Here we only consider the case of neutrally stable conditions (no density stratification by heat and moisture). In those circumstances the wind profile has a logarithmic height dependence

$$U_0(z) = \frac{u_*}{\kappa} \ln\left(1 + \frac{z}{z_0}\right), \quad (80)$$

which follows from the condition that the momentum flux in the surface layer is constant for steady conditions. This profile depends on three parameters. The von Karman constant κ is supposed to be universal (we take the value $\kappa = 0.41$), the friction velocity u_* is a measure of the momentum flux and z_0 , the so-called roughness length, is a parameter which reflects the loss of momentum to the sea surface. In the past, the roughness length has been determined empirically. Over sea a good choice is the one proposed by Charnock (1955)

$$z_0 = \alpha u_*^2 / g \quad (81)$$

with α the so-called Charnock parameter. Here, for now we assume that α is a constant, we take $\alpha = 0.0144$,

although there are arguments that α is not a constant but depends on the sea state.

Given the wind profile (80) we can no solve (74) numerically and use the result for χ at the critical height to evaluate the growth rate from Eq. (79). With $f = \omega/2\pi$, the numerical results for the dimensionless growth rate $2\gamma_a/f = \gamma/f$ are plotted as a function of u_*/c in Fig. 5 (note: the growth rate of the energy of a wave is $2\gamma_a$ as the energy is proportional to the square of the amplitude). For comparison, we have also shown measurements of wave growth from the field (Snyder et al., 1981) and the laboratory (Plant and Wright, 1977). It is concluded that there is a fair agreement between Miles' theory and observations.

We may summarise the results for wind–wave generation obtained thus far by noting that we have determined the rate of change of the amplitude of a gravity wave due to wind. The growth rate, giving in Eq. (79), is proportional to the air water density ratio and is a sensitive function of the dimensionless frequency $u_*/c = u_*\omega/g$. In fact, the short waves have the largest relative growth rate, as may be inferred from Fig. 5.

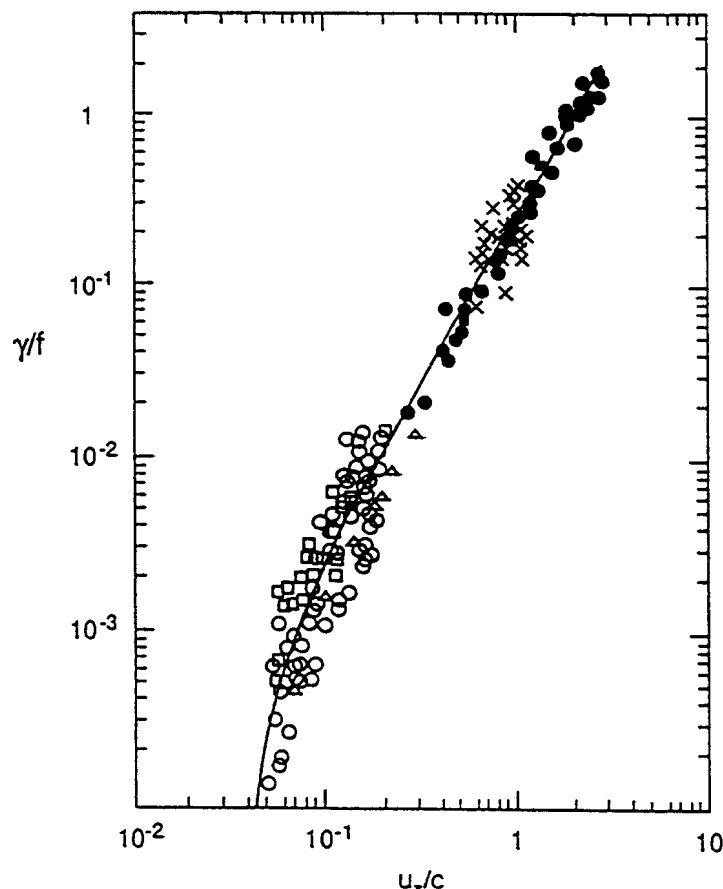


Figure 5. Wave growth versus phase speed; comparison of Miles' theory and observations.

Our results may be immediately generalised to the case of a continuous spectrum. The wind input source term of the action balance equation (45) therefore becomes

$$\left. \frac{\partial N}{\partial t} \right|_{\text{wind}} = 2\gamma_a N \quad (82)$$

where the growth rate γ_a is given by Eq. (79).



Before we proceed to a discussion of the non-linear interaction source term, we would like to return to the issue of the slowing down of the air flow because of the growing gravity waves. It was mentioned that, for a single wave, the force imposed by the wave on the air flow would be a delta function in height (z)-space. In reality, one deals, however, with a continuum of ocean waves. Consequently, one deals with a continuum of critical layers and the force exerted by a continuum of ocean waves on the mean air flow is therefore a 'nice'-smooth function of height. Thus, the rate of change of the mean flow $U_0(z, t)$ due to a spectrum of growing surface gravity waves follows from

$$\frac{\partial}{\partial t} U_0|_{\text{waves}} = \frac{\partial}{\partial z} \tau_w(z, t) \quad (83)$$

where the wave-induced stress is defined as

$$\tau_w = -\langle \delta u \delta w \rangle \quad (84)$$

and δu and δw denote the wave-induced horizontal and vertical velocities in the air. These quantities are known, even for a continuum, when the solution of Rayleigh's equation is known. The result is an equation for the mean flow U_0 which is of the diffusion type

$$\frac{\partial}{\partial t} U_0|_{\text{waves}} = D_w \frac{\partial^2}{\partial z^2} U_0 \quad (85)$$

where the wave diffusion coefficient D_w is proportional to the action density spectrum N ,

$$D_w = \frac{\pi c^3 k^3 |\chi|^2}{|c - v_g|} N(k) \quad (86)$$

Here, the wave number k has to be expressed as a function of height through the resonance condition $W_0 = 0$. In passing, we remark that (85)–(86) is only valid for dispersive waves for which $c \neq v_g$. Since the wave diffusion coefficient D_w is positive, we immediately conclude that ocean waves give rise to a slowing down of the air flow. This slowing down depends, in a sensitive manner, on the sea state; it depends in particular on the high-wave number spectrum because these waves grow the fastest. In Fig. 6 we show the equilibrium wind speed profile for two different sea states, which are termed 'old' and 'young' wind sea. For old wind sea the ocean waves have reached an equilibrium with the wind and the high wave number part of the spectrum has a small steepness. Young wind sea, on the other hand, have just been generated by the wind and have a large steepness. As a consequence, we see that, for young waves, there is a considerable slowing down of the wind. In fact, one may obtain the Charnock parameter from Fig. 6 by searching for the intercept of the wind profile with the x -axis (which is normalised height gz/u_*^2). It is then seen that the Charnock parameter for old wind sea is about 0.014 while, for young wind sea, it is 10 times as large. Consequences of the sea state dependence of the Charnock parameter on, e.g., atmospheric flow will be discussed in 3.2. This is important as atmospheric models used to assume a constant Charnock parameter α (typically $\alpha \approx 0.018$).

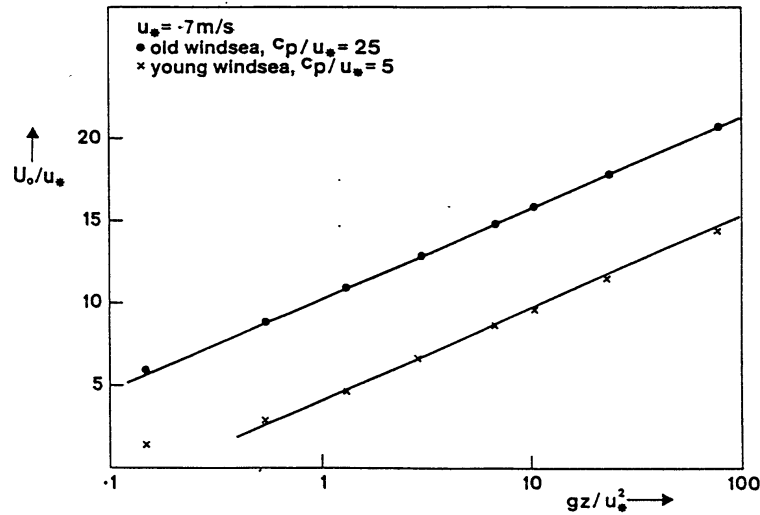


Figure 6. Wind speed as function of height for young and old wind sea.

Non-linear transfer

The study of the effects of non-linearity on deep-water gravity waves already started in the last century with the great contribution of Stokes (1849). He considered a single wave of permanent shape and was able to find the effects of finite wave amplitude on the dispersion relation by means of a so-called singular perturbation technique. A century later, Lighthill (1965) discovered that a non-linear water wave is unstable to modulational perturbations, giving a transfer of energy from the basic wave to sidebands. This instability is a special case of a four wave interaction process, which nowadays plays a major role in the physics of ocean waves. The instability is now known as the Benjamin–Feir instability, because Benjamin and Feir were the first to give experimental evidence for its existence.

These discoveries lead to a lot of excitement in the field of non-linear waves and, in particular, the contributions of the 'California' school may be mentioned. Yuen and Lake investigated the long term behaviour of the unstable wave train and they found that the wave train did not disintegrate, but instead it recurred after a finite time to its original shape (however with slightly lower frequency of the wave train).

All these exciting results were obtained in the context of deterministic evolution equations. In a statistical framework all these phenomena seem to be less relevant. The reason for this is that such non-linear effects depend, in a sensitive manner, on the phases of the waves involved in the non-linear interaction. In a statistical approach all these effects are then washed away because of the random independent phases.

We therefore only concentrate on the statistical framework, but we briefly describe how to obtain the deterministic evolution equation from the Hamiltonian for water waves. These equations are then used as a starting point for the statistical theory.

In deep water the energy density of the waves is

$$\varepsilon = \frac{1}{2}\rho \int_{-\infty}^{\eta} dz \{(\nabla\phi)^2 + \phi_z^2\} + \frac{1}{2}\rho g \eta^2 \quad (87)$$

and we express the potential ϕ in terms of the canonical variables η and $\psi(\mathbf{x}, t) = \phi(\mathbf{x}, \eta, t)$ by solving the potential problem

$$\begin{aligned}
 \Delta\phi + \phi_{zz} &= 0 \\
 z = \eta, \quad \phi &= \psi \\
 z = -\infty, \quad \phi_z &= 0
 \end{aligned} \tag{88}$$

in an iterative fashion by assuming small amplitude waves with small wave steepness. This is most conveniently done by using Fourier transformation of surface elevation η and ψ . A great simplification is then achieved by introducing the complex action-variable $a(\mathbf{k})$ through

$$\begin{aligned}
 \hat{\eta}(\mathbf{k}) &= \frac{1}{\sqrt{2}} \left(\frac{k}{\omega} \right)^{1/2} [a(\mathbf{k}) + a^*(-\mathbf{k})] \\
 \hat{\psi}(\mathbf{k}) &= \frac{-i}{\sqrt{2}} \left(\frac{\omega}{k} \right)^{1/2} [a(\mathbf{k}) - a^*(-\mathbf{k})]
 \end{aligned} \tag{89}$$

where $\omega(k)$ is just the dispersion law for gravity waves

$$\omega(k) = \sqrt{gk}$$

After having obtained the potential ϕ to any required order of wave amplitude, one may determine the energy of the wave system, thus

$$E = \int dx \varepsilon = \int d\mathbf{k}_1 \omega_1 a_1 a_1^* + \int d\mathbf{k}_1 d\mathbf{k}_2 d\mathbf{k}_3 \delta(\mathbf{k}_1 - \mathbf{k}_2 - \mathbf{k}_3) V_{1,2,3} [a_1^* a_2 a_3 + \text{c.c.}] + \text{LOT} + O(a^4) \tag{90}$$

where we introduced the shorthand notation $a_1 = a(\mathbf{k}_1)$, etc and V is a known function of wave number. Furthermore, LOT is an abbreviation for lots of other terms. We recognise the first term as being the energy for a single wave, while the cubic term represents the lowest-order non-linear effect on the energy.

The introduction of the complex action variable $a(\mathbf{k})$ has the additional advantage that Hamilton's equations (10), i.e.

$$\frac{\partial \eta}{\partial t} = \frac{\delta E}{\delta \psi}, \quad \frac{\partial \psi}{\partial t} = -\frac{\delta E}{\delta \eta}$$

become the single equation

$$\frac{\partial}{\partial t} a(\mathbf{k}) = -i \frac{\delta E}{\delta a^*} \tag{91}$$

Evaluating the functional derivative of E with respect to a^* then gives the deterministic evolution equation for a

$$\begin{aligned}
 \frac{\partial}{\partial t} a_1 + i\omega_1 a_1 &= -i \int d\mathbf{k}_2 d\mathbf{k}_3 V_{1,2,3} a_2 a_3 \delta(\mathbf{k}_1 - \mathbf{k}_2 - \mathbf{k}_3) + \dots + \\
 &-i \int d\mathbf{k}_2 d\mathbf{k}_3 d\mathbf{k}_4 W_{1,2,3,4} \delta(\mathbf{k}_1 + \mathbf{k}_2 - \mathbf{k}_3 - \mathbf{k}_4) a_2^* a_3 a_4
 \end{aligned} \tag{92}$$

where V and W are known functions of wave number.

The non-linear evolution equations (92) contain the effects of three and four wave interactions. To see this, we recall that (92) was obtained under the assumption of small wave steepness so that, in lowest order, we are dealing

with a linear oscillation and the right hand side (RHS) gives small (but important) corrections to this linear oscillation. Now consider the quadratic terms on the RHS of (92). I have not shown all of them, but the one given explicitly, oscillates with frequency $-(\omega_2 + \omega_3)$, while the others that are not shown oscillate as $-\omega_2 + \omega_3$ and $\omega_2 + \omega_3$. If they match the oscillation frequency $-\omega_1$ of the linear system, a resonant energy transfer between the modes with wave numbers \mathbf{k}_1 , \mathbf{k}_2 and \mathbf{k}_3 is possible. Likewise, the cubic terms oscillate with frequency $\omega_2 - \omega_3 - \omega_3$ and, if this frequency equals $-\omega_1$ of the linear system, a resonant interaction between four modes occurs [note, however, that the quadratic terms also contribute to four wave interaction].

To summarise, the evolution equation (92) allows both three- and four-wave interactions, where for three-wave processes the resonance conditions

$$\omega_1 \pm \omega_2 \pm \omega_3 = 0, \quad \mathbf{k}_1 \pm \mathbf{k}_2 \pm \mathbf{k}_3 = 0 \tag{93}$$

should be satisfied simultaneously, and for four wave processes the resonance conditions

$$\omega_1 + \omega_2 - \omega_3 - \omega_4 = 0, \quad \mathbf{k}_1 + \mathbf{k}_2 = \mathbf{k}_3 + \mathbf{k}_4 \tag{94}$$

should be satisfied. Whether these resonance conditions can actually be satisfied depends on the type of dispersion relation, $\omega = \omega(k)$. Now, gravity waves have the dispersion relation $\omega = \sqrt{gk}$ and, from a graphical construction, one immediately concludes that three-wave processes are impossible.

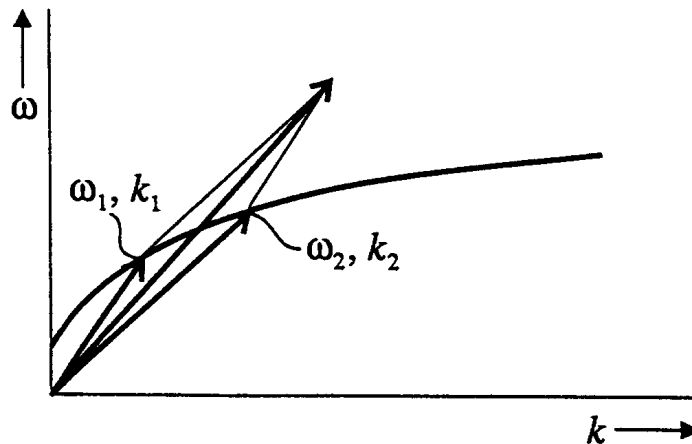


Figure 7. Three wave interaction is impossible for gravity waves.

Phillips (1960) has shown, however, that four-wave interactions are permitted by the deep-water dispersion relation. The possible solutions are sketched in Fig. 8, which has become known as Phillips figure of eight.

Let us finally try to determine from Eq. (92) the statistical evolution of the action density due to four-wave processes. Since the mean of the surface elevation vanishes, $\langle a_1 \rangle = 0$, our aim now is to derive an evolution equation for the second moment $\langle a_1 a_2^* \rangle$. Here the brackets denote, as before, an ensemble average. Owing to non-linearity, the development of the second moment is determined by the third and the fourth moment, and so on. As a result we find an infinite hierarchy of equations, and the question is how to truncate this hierarchy. A meaningful truncation is now obtained by making two assumptions, namely we assume that, on the scale of the wavelength, the ensemble of waves is spatially homogeneous and that the probability distribution for a_1 is close to a Gaussian.

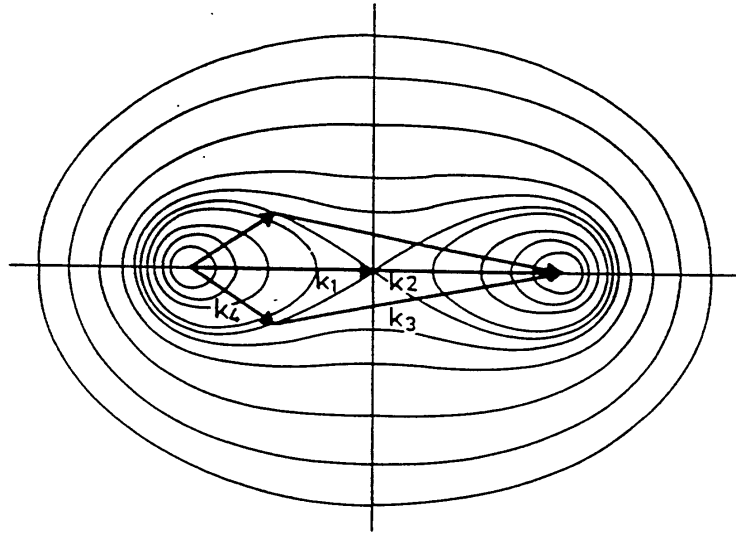


Figure 8. Phillips' figure of 8.

We shall not give the details of how to obtain the rate of change of the action density due to non-linear interactions. We merely point out that, by means of the above assumptions, this is indeed possible. Details of its derivation may be found in [Hasselmann \(1962\)](#), [Davidson \(1972\)](#) and [Komen *et al.* \(1994\)](#). The eventual result is

$$\left. \frac{\partial N_1}{\partial t} \right|_{\text{nonlin}} = 4\pi \int d\mathbf{k}_2 d\mathbf{k}_3 d\mathbf{k}_4 T_{1,2,3,4}^2 \delta(\mathbf{k}_2 + \mathbf{k}_3 - \mathbf{k}_4 - \mathbf{k}_1) \delta(\omega_2 + \omega_3 - \omega_4 - \omega_1) \times \{N_2 N_3 (N_1 + N_4) - N_1 N_4 (N_2 + N_3)\} \quad (95)$$

Here, T depends on V and W . For gravity waves this evolution equation was first obtained by [Hasselmann \(1962\)](#).

In the remaining part of the section we shall discuss some general properties of [Eq. \(95\)](#) (I personally call it the Hasselmann equation).

(a) N never becomes negative

The Hasselmann equation has the property that it can never give rise to negative action densities. Before a density becomes negative, it must first become zero. But for zero N the second factor between curly brackets vanishes while the first factor is positive. Thus, $\partial N / \partial t$ is positive, and N will become positive rather than negative.

(b) Conservation laws

The Hasselmann equation admits conservation of

- action: $\int d\mathbf{k} N(\mathbf{k})$
- momentum: $\int d\mathbf{k} \mathbf{k} N(\mathbf{k})$

and

- energy: $\int d\mathbf{k} \omega N(\mathbf{k})$.

This means that a wave field cannot gain or lose energy through the four-wave interaction. Growth or dissipation of wave action, momentum or energy must, therefore, take place through other processes, such as wind input or white capping.

(c) Implications for energy transfer

The conservation of two scalar quantities, energy and action, implies an important general property of the energy transfer. A similar relation holds for the energy transfer in a two-dimensional turbulence spectrum in the atmosphere, which also conserves two scalar quantities, namely energy and enstrophy.

The one-dimensional energy transfer $dN(\omega)/dt$ must have at least three lobes of different sign (cf Fig. 9).

It cannot have a two-lobe structure representing, for example, an energy cascade from low to high frequencies, as in three-dimensional turbulence. The ratio energy/action = ω increases monotonically with frequency. Thus, if the net action lost in the negative low-frequency lobe balances the action gained in the high-frequency lobe, the energy loss in the low-frequency lobe must necessarily be smaller than the energy gained in the high-frequency lobe, so that energy is not conserved. Numerical computations of the non-linear energy transfer indeed give the three-lobe structure. In particular, it should be pointed out that the positive lobe at low frequencies has important consequences for the evolution of the wave spectrum as it gives rise to the shift of spectrum towards lower frequencies.

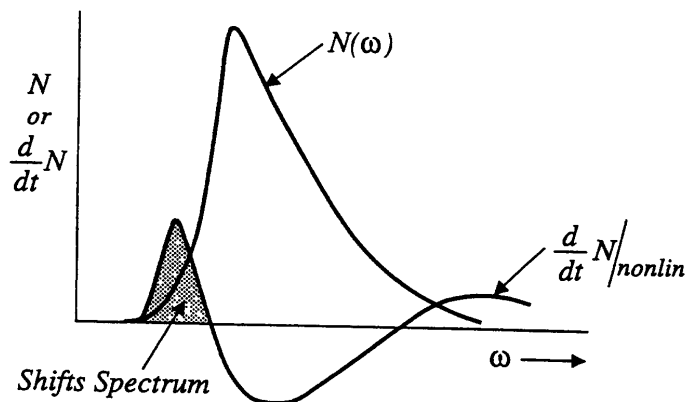


Figure 9. One-dimensional energy transfer caused by 4-wave interaction.

Dissipation due to wave breaking

The least understood aspect of the physics of wave evolution is the dissipation source function. Waves may lose energy continuously by viscous dissipation and by the highly intermittent process of wave breaking. The continuous slow drain of wave energy by viscosity is well understood and easily calculated. While it is an important sink for gravity–capillary waves, with wavelengths of the order of 1 cm, it is insignificant for the longer waves.

Understanding and modelling the wave breaking process is thus of critical importance in achieving an accurate representation of the principle sink function in the action balance equation. Unfortunately, there has not been much progress in obtaining a convincing model of dissipation caused by wave breaking. Nevertheless, one could hope that this goal may be achieved in the future because, although wave breaking is a truly non-linear phenomenon, it occurs only relatively rarely (say at best 5% of the waves are involved breaking). In the context of a statistical theory of wave evolution, dissipation due to wave breaking, therefore, should have a relatively small effect. Following this line of approach, Hasselmann (1974) obtained some general constraints on the form of the dissipation source function. Introducing the mean frequency $\langle \omega \rangle$ and mean wave number $\langle k \rangle$,

$$\langle \omega \rangle = \frac{\int dk \omega N}{\int dk N}$$

and a similar relation for $\langle k \rangle$, Hasselmann (1974) proposed the following dissipation source term

$$S_{\text{dissip}} = -\beta \langle \omega \rangle (\langle k \rangle^2 m_0)^2 [(1 - \delta)x + \delta x^2] N \quad (96)$$

where $x = k / \langle k \rangle$, $m_0 = \langle \eta^2 \rangle$ is the wave variance, and β and δ are constants.

It is emphasized that this dissipation source term has a quasi-linear shape. It is linear in the action density, but the proportionality constant depends on integrals over the wave spectrum. We finally remark that (96) is in agreement with one's intuition that the dissipation is larger for steeper waves since S_{dissip} is proportional to the integral steepness parameter $\langle k \rangle^2 m_0$. Furthermore, the constant's β and S are unknown and will be used as tuning constants (cf next section).

2. THE WAM MODEL

The WAM model is the first model that solves the complete action density equation, including non-linear wave-wave interactions. A group of European waves modellers, who called themselves the WAM group, realised in the middle of the 1980's that it should be feasible to develop a wave model on first principles. First of all, there was a clear need for improving existing wave models at that time. Although these models performed reasonably well in many cases, it turned out that, in rapidly varying circumstances, these models simply failed to give a proper description of the sea state. This followed from a comparison exercise where about 10 different models were run with the same hurricane wind field, resulting in widely varying maximum wave height (ranging from 8 to 25 m). Secondly, the solution of the energy balance equation requires considerable computing power which has become available in recent years. Thirdly, this coincided with the development of remote sensing techniques for measurements of the sea surface by means of microwave instruments (altimeter, scatterometer and synthetic aperture radar (SAR)). The relationship between wave-model development and satellite remote sensing is much closer than one might expect at first sight. Satellite observations can be used to validate the model and the model also gives a first check on the accuracy of the observations. Furthermore, a detailed description of the dynamics of the sea surface is important for a correct interpretation of the radar signals.

At present, the WAM model is used operationally in global and regional applications to make forecasts of the sea state, which can be used for many applications such as ship routing and offshore activities, and for the validation and interpretation of satellite observations. Finally, much progress has been made on the assimilation of satellite observations into wave models. Deviations between predicted and observed waves are normally indicators of errors in the driving wind fields so that effective wave data assimilation procedures correct both wind and wave fields.

In the next sections we will present results of the WAM model in simple situations, such as growth of waves under fetch limited circumstances, and compare results with in-situ campaigns. Subsequently, we discuss the quality of the wave analysis and wave forecast for the global area.

2.1 Energy balance for wind sea

Since the Second World War one has attempted to summarise knowledge of the growth of ocean waves by wind in terms of empirical growth curves. In principle, a large number of variables may control wave growth. For example, in the idealised situation of duration-limited waves (when a uniform and steady wind has been blown over an unlimited ocean for time t after a sudden onset) the following variables should be considered: frequency ω , wind-

speed U_{10} or friction velocity u_* , acceleration of gravity g , viscosity, surface tension, air and water density and coriolis parameter f . In principle, U_{10} is supposed to represent the wind at infinite height (the geostrophic wind). In practice, U_{10} is the speed at 10 m height and may not always be appropriate as speed scale.

Under assumptions of the nature of the wave motion and the mechanism of the wave growth, the energy containing part of the spectrum is mainly determined by the variables ω , U_{10} (or u_*), g , t . We remark that, according to theory, the friction velocity u_* is probably the most appropriate parameter to use in scaling wave growth. However, since this parameter is so difficult to measure in practice, one normally uses the wind at 10 m height.

Conditions of duration-limited growth are difficult to fulfil in practice and, from the point of view of the analysis of experimental data, two other idealized cases are more important. One is the case of fully developed waves, when a uniform and steady wind has blown over an unlimited ocean long enough for the wave field to become independent of time. This may occur in the Trade Winds. The other, more frequently occurring, situation is the fetch-limited case, when a uniform steady wind has blown from a straight shoreline long enough for the wave field at distance (fetch) X from the upwind shore to become independent of time.

Let us now make the connection between what we have developed in the previous section and the experimental practice. We have obtained the evolution equation for the action density $N(\mathbf{k})$ which is related to the wave number spectrum through

$$F(\mathbf{k}) = \sigma N(\mathbf{k}).$$

Here, the wave-number spectrum is normalised with the variance $\langle \eta^2 \rangle$, where η is the surface elevation,

$$\int d\mathbf{k} F(\mathbf{k}) = \langle \eta^2 \rangle = m_0.$$

Obviously, the integral over the wave spectrum has dimension of a length square and it is then common to introduce the significant wave height H_s according to

$$H_s = 4\sqrt{\langle \eta^2 \rangle} \quad (97)$$

The reason for this definition is historical. In the early days one could not measure the wave spectrum and therefore the wave height $H_{1/3}$ was observed visually. The measure $H_{1/3}$ is defined as the average height of the highest 1/3 of the waves, and it can be shown that approximately $H_s = H_{1/3}$. For a narrow spectrum $H_{1/3}$ and H_s are exactly equal.

In situ observations of the two-dimensional wavenumber spectrum are rare; it requires rather sophisticated instrumentation to observe the spatial correlation function. Therefore, in routine operations one normally observes the frequency spectrum which just requires the analysis of time series. The frequency spectrum is defined as

$$F_2(\omega, \theta) d\omega d\theta = F(\mathbf{k}) d\mathbf{k} = F(k, \theta) k dk d\theta$$

thus

$$F_2(\omega, \theta) = \frac{k}{v_g} F(k, \theta) \quad (98)$$

Even the directional properties of waves require expensive buoys and, for this reason, one also has introduced the one-dimensional frequency spectrum,

$$F_1(\omega) = \int d\theta F_2(\omega, \theta) \quad (99)$$

As long as there is no confusion we shall use the same symbol for the various forms of the wave spectrum, namely F ; the distinction should be clear from their arguments, $F(\mathbf{k})$, $F(\omega, \theta)$ and $F(\omega)$.

Let us now return to the analysis of wave evolution. For fully developed waves one would therefore expect that the following relations hold

$$\begin{aligned} g^3 F(\omega)/U_{10}^5 &= f(\omega U_{10}/g) \\ g^2 m_0/U_{10}^4 &= \text{constant} \\ \omega_p U_{10}/g &= \text{constant} \end{aligned} \quad (100)$$

Here, m_0 is the total wave variance and ω_p denotes the peak of the frequency spectrum. On the other hand, in fetch-limited conditions one would expect the relation

$$\begin{aligned} g^3 F(\omega)/U_{10}^5 &= f(\omega U_{10}/g, gX/U_{10}^2) \\ g^2 m_0/U_{10}^4 &= f(gX/U_{10}^2) \\ \omega_p U_{10}/g &= f(gX/U_{10}^2) \end{aligned} \quad (101)$$

In cases where measurements of the friction velocity u_* have been performed it seems appropriate to replace U_{10} by u_* . The above similarity laws are due to [Kitaigorodskii \(1962\)](#).

[Figs. 10 and 11](#) give a brief summary of results obtained by a number of field campaigns in the past. [Fig. 10](#) shows the evolution of dimensionless wave variance and peak frequency as function of dimensionless fetch, while [Fig. 11](#) shows the evolution of the wave spectrum with fetch according to [JONSWAP \(1973\)](#).

Before we discuss results obtained with the WAM model we have to point out the important distinction between wind sea and swell. Thus far we only considered wind sea. Loosely speaking one may define as wind sea that part of the wave spectrum that is under direct influence of the wind. All the ideal cases discussed so far are examples of wind sea. However, a storm has only a finite extent. Although ocean waves suffer from dissipation due to wave breaking, when their steepness is small enough there is hardly any dissipation. Therefore, ocean waves may propagate freely over large distances. A well-known example is that of [Snodgrass et al. \(1966\)](#) who observed waves generated in the Gulf of Alaska to propagate all the way to the Indian Ocean. Those waves that are not under the direct influence of the wind are called swell. Wind sea is usually found in the areas of large wind, such as the storm tracks. When these wind waves leave the storm track they become swell and, in practice, the sea state in the tropical oceans is dominated by swell.

Let us now discuss the performance of the WAM model. To that end we first of all compare results of fetch-limited runs with the JONSWAP data. Next, some interesting results of duration-limited cases are shown.

[Figs. 12 and 13](#) show results of the fetch-limited cases and the comparison with the JONSWAP fetch-laws. In order to show the sensitivity of wave model results to differences in wind speed, in the figure for the dimensionless growth curve we display two cases, namely $U_{10} = 18$ m/s and $U_{10} = 8$ m/s. The JONSWAP experiment was performed for an average wind speed of 8–9 m/s and, therefore, there is a fair agreement with the JONSWAP observation. The same holds for the dimensionless peak frequency.

We remark that, according to the WAM model, there is no universal scaling when wave results are scaled in terms of the wind speed at 10 m height. The reason for this is easily understood. From the previous section we have seen

that the wind-input term scales with the friction velocity and not with the wind speed at 10 m height. For air flow over the ocean, the ratio of friction velocity to wind speed at a certain height depends on that very wind speed and, thus, it makes a difference when one uses friction velocity or wind speed. In order to show this last point, we take the opportunity to introduce the drag coefficient C_D , defined as

$$C_D = \frac{\tau}{U_{10}^2}, \quad \tau = u_*^2 \quad (102)$$

and, by using the logarithmic wind profile (Eq. (80)), one finds

$$C_D = \left\{ \frac{\kappa}{\ln(10/z_0)} \right\}^2 \quad (103)$$

where z_0 is the roughness given by the Charnock relation. It is important to note that z_0 depends on the friction velocity and, therefore, C_D (and u_*/U_{10}) depends on wind speed. The important consequence is, therefore, that, when scaling in terms of U_{10} is performed, a family of growth curves is found as we have seen in Fig. 12. It should be realised by now that it is not appropriate to scale wave results with U_{10} because the 10 m height is really arbitrary and bears no relation to any length scale in the physical system. On the other hand, it should be pointed out that in the past there was no other choice because the friction velocity u_* was too difficult to measure.

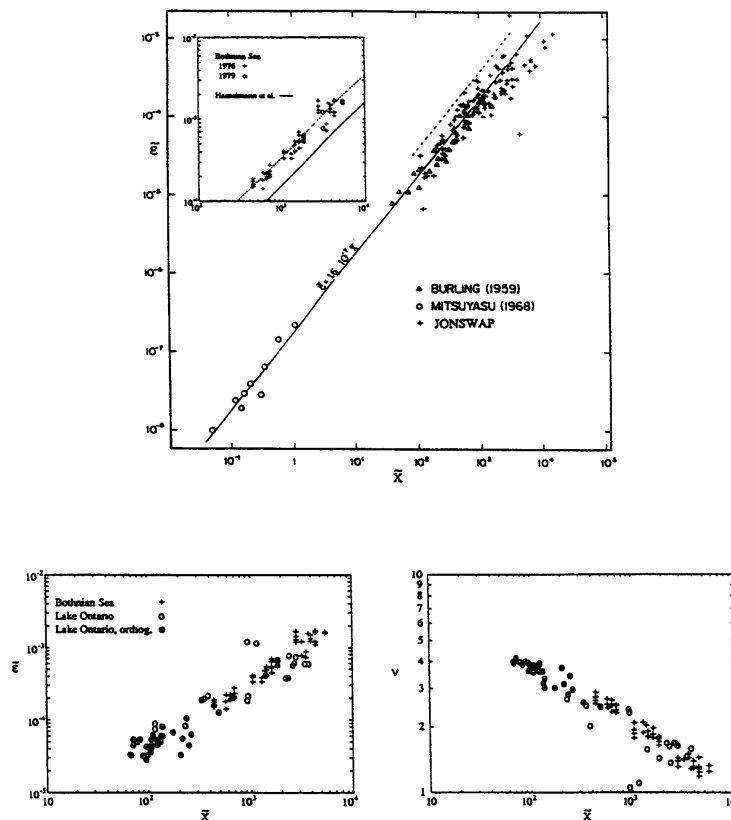


Figure 10. Examples of fetch-limited growth curves for energy and peak frequency.

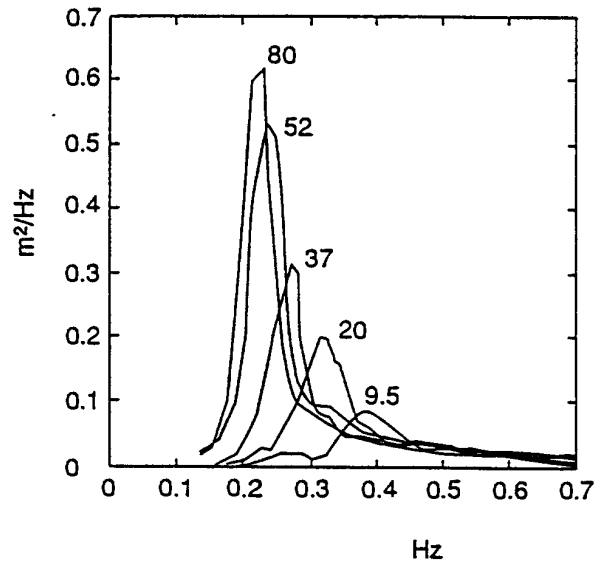


Figure 11. Evolution of wave spectra with fetch for offshore winds (11-12 h, 15 Sept 1968). The spectra are labelled with the fetch in kilometres. (From Hasselmann *et al.*, 1973).

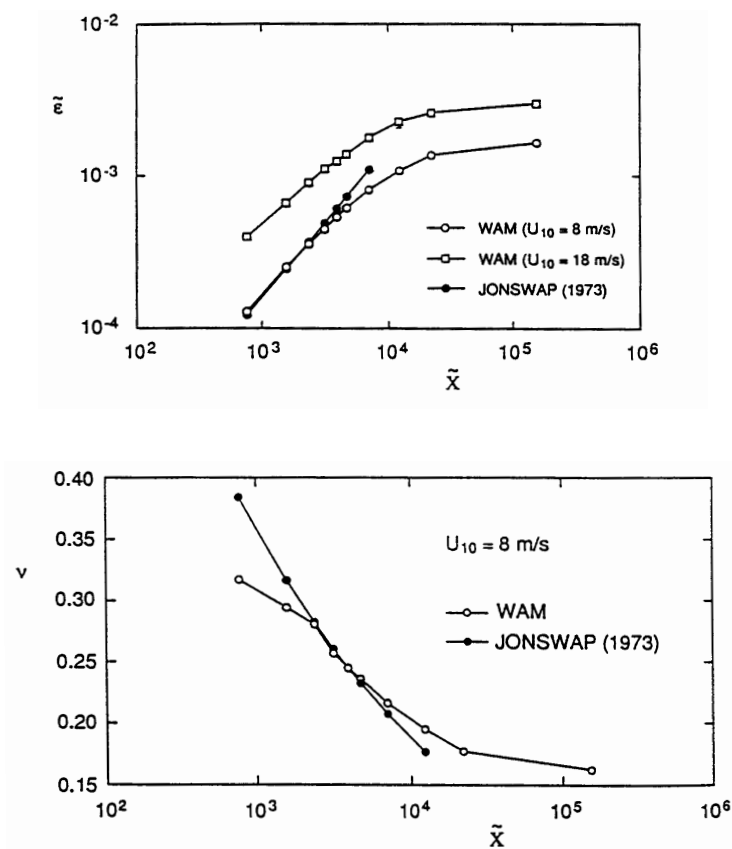


Figure 12. Fetch dependence of dimensionless energy and peak frequency for a wind speed of 8 m/s. JONSWAP fetch laws are shown as well.

Fig. 13 shows the comparison of modelled and observed evolution of the so-called Phillips 'constant' α_p . As may be noted, this parameter is not really a constant. Here it is defined as the average of $\omega^5 F(\omega)/g^2$ over the frequency range between 1.3 and 2.5 times the peak frequency. The Phillips constant has played a role in discussions on wave evolution because it was thought at the time that in this frequency range the frequency spectrum has a ω^{-5} power law. Nowadays, opinions differ on this matter, but in the high-frequency range with $\omega > 3\omega_p$ this certainly gives a useful description of the wave spectrum. In any event, this quantity may be regarded as a measure of steepness of the high-frequency waves and the agreement between the observed and modelled Phillips constants seems fair. Note that for short fetches (young wind sea) the steepness of the waves is much larger than for long fetches (old wind sea).

In order to conclude this section we would like to discuss results of duration-limited cases. Thus, we consider an infinite ocean and consider the evolution in time of the waves. These results can easily be obtained by taking a single grid-point model and switching off the advection. It is feasible to run this model on a PC.

According to our results regarding the wind-input source term, the surface stress depends on the sea state, giving a much rougher flow for young wind sea than for old wind sea. For young wind waves one would, therefore, expect a slowing down of the air flow. A proper description of this deceleration of the flow may, however, only be accomplished in a coupled atmosphere/ocean-wave model. Such tests cannot be regarded as straightforward and, since we would like to concentrate here on aspects of the wave physics, we shall make the simplifying assumption that the wind speed is constant. The wind speed U_{10} was chosen to be 18 m/s, corresponding, in the absence of waves, to a friction velocity u_* of 0.85 m/s (with Charnock parameter $\alpha = 0.0185$). Results with a coupled atmosphere, ocean-wave model are discussed in section 3.2.

The first experiment which we performed was a reference run with the wave model without any coupling between wind and waves. This was achieved by simply disregarding the effect of waves on the roughness (called 'uncoupled' in the following figures). Next, we coupled the waves and the air flow as is done in the WAM model. The effect of the waves on the air flow was modelled by allowing the Charnock parameter to depend on the wave-induced stress τ_w . Details of this model are given in Komen *et al.* (1994). The results for the coupled run are labelled by 'coupled'.

We infer from Figs. 14–17 that the coupling between wind and waves has a small impact on wave height, a somewhat bigger impact on the wave-induced stress and a dramatic impact on the evolution of the drag coefficient C_D (of course, for the control run C_D is a constant). This shows that the drag coefficient depends on the sea state, which is caused by the sea-state dependence of the wave-induced stress. This latter feature is in turn caused by the time dependence of the Phillips' constant α_p .

Furthermore, we show the evolution in time of the frequency spectrum in Fig. 18. In the course of time the wave spectrum shows a typical shift of the peak of the spectrum towards lower frequencies, while a considerable enhancement of the peak of the spectrum is also noticed in the early stages of wave growth. In hindsight it may be noted that it was the peak enhancement which assured that the non-linear interactions were found to be relevant (a factor of 2 in the peak of the spectrum already gives a factor of 8 in the rate of change of the non-linear transfer). In Figs. 19–20 we show the energy balance of young ($T = 3$ h) and old ($T = 96$ h) wind sea. Wind input and dissipation behave as expected. The non-linear transfer has a typical three-lobe structure and the first lobe causes the shift in the peak of the spectrum. We have also given the total source term, which is the sum of wind input, non-linear transfer and dissipation. While for young wind sea there are clear signs that the sea state is not in equilibrium with the wind, for old wind sea (after 96 h) the steady state is almost reached.

Finally, in order to show how the two-dimensional wave spectrum evolves in time, in Fig. 21 we have shown results with the single grid point version of the WAM model for a turning wind field case. Wind speed was again 18 m/s. The arrow shows the wind direction.

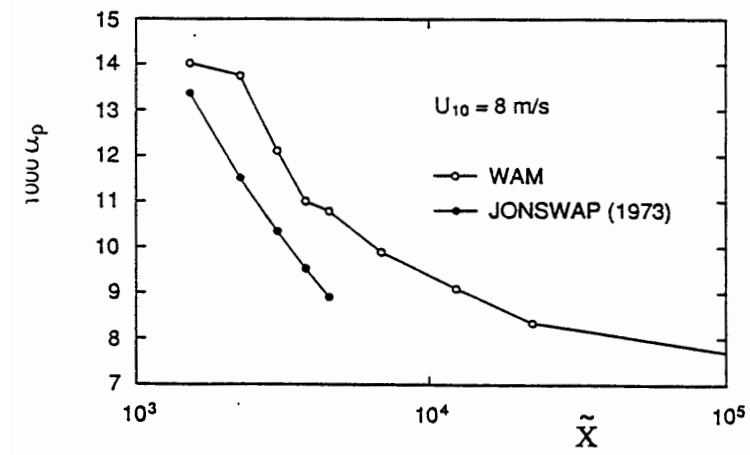


Figure 13. Fetch dependence of Phillips' parameter α_p . The JONSWAP fetch law is plotted as well.

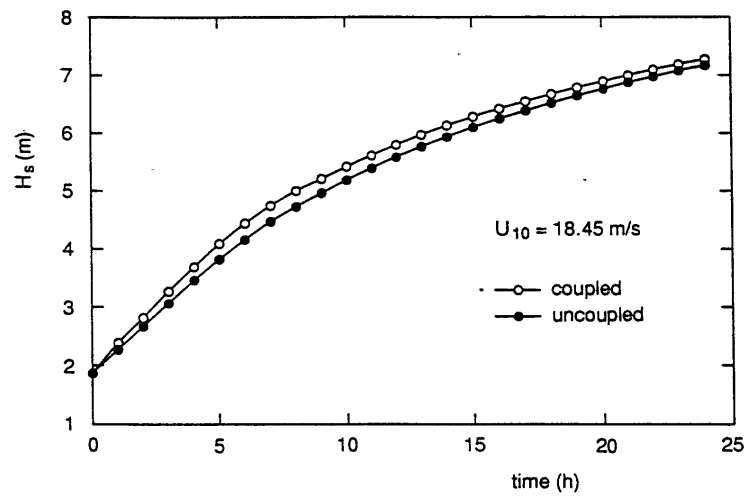


Figure 14. Time dependence of wave height for coupled and control run.

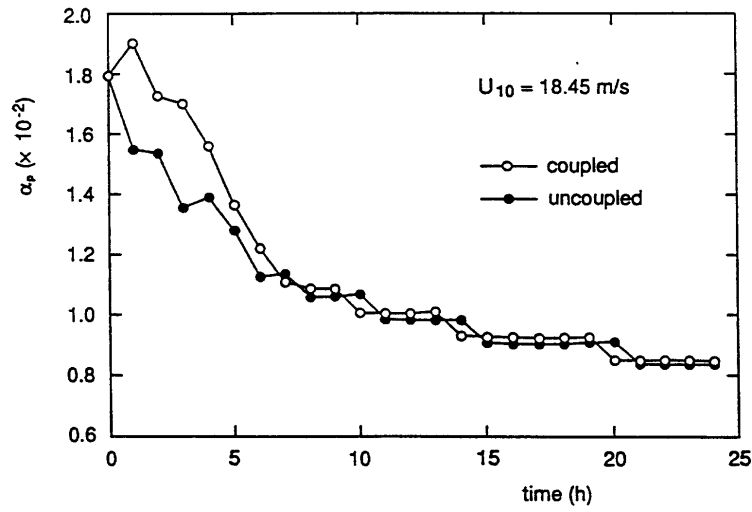


Figure 15. Time dependence of Phillips' parameter α_p for a reference run and a coupled run.

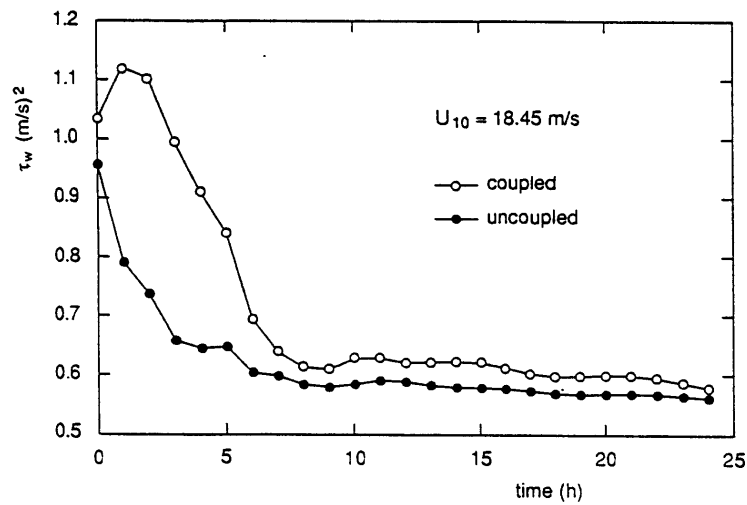


Figure 16. Time dependence of wave-induced stress for a reference run and a coupled run.

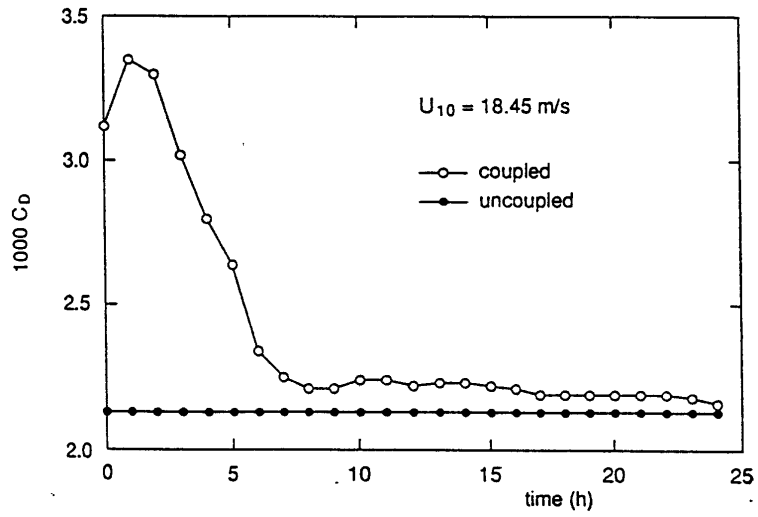


Figure 17. Time dependence of drag coefficient C_D for a reference run and a coupled run.

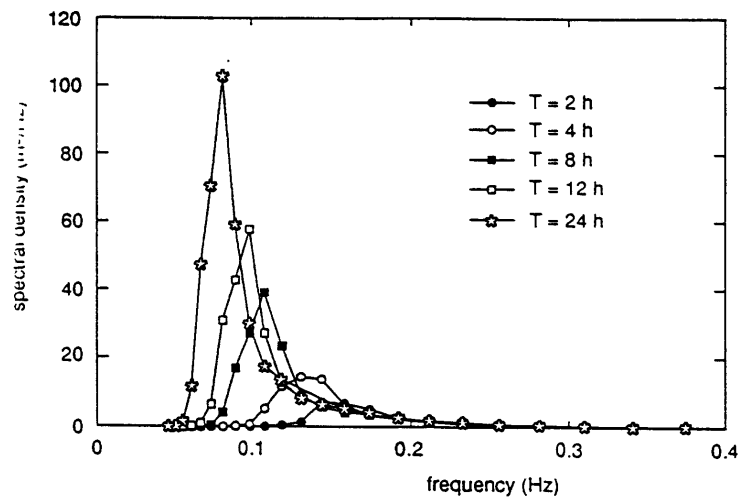


Figure 18. Evolution in time of the one-dimensional frequency spectrum for the coupled run.

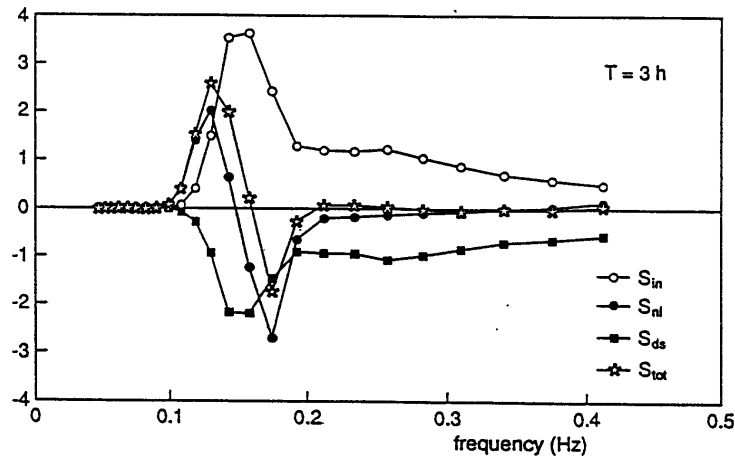


Figure 19. The energy balance for young duration-limited wind sea.

2.2 Wave forecasting

I would like to start this section with a brief discussion of the sensitivity of wave results to errors in the driving wind field by means of a single illustrative example. Next, I would like to discuss how the quality of the wave analysis is monitored by comparing the wave height field with observations from the ERS-1 altimeter and with buoy data. Of course, the surface winds are validated in a similar fashion. Finally, I will describe how we attempt to investigate the quality of the wave forecast and the forecast skill.

Presently, we have two operational implementations of the WAM model here at ECMWF. One is a global model with 0.5° resolution, the other is a limited-area version covering the North Atlantic and the European seas with a 0.25° resolution. The spectrum is discretized in 30 frequency bins and 24 directions. The integration time step is typically 15 min. The WAM model is a fully vectorised code, which can be run in parallel mode.

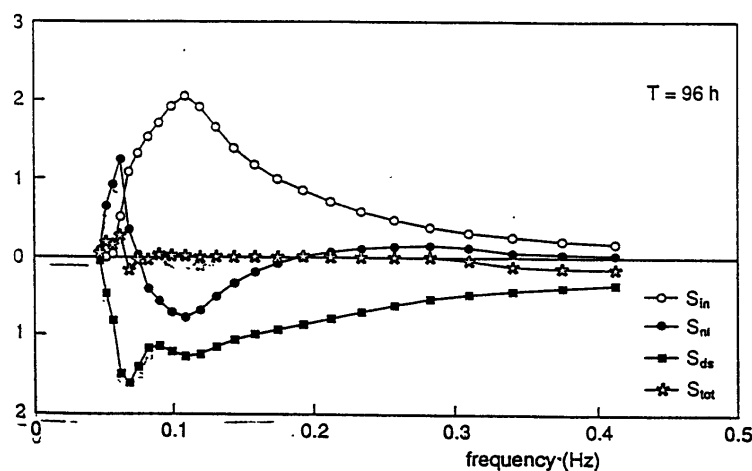


Figure 20. The energy balance for old wind sea.

Sensitivity to wind field errors

A well-known rule of thumb in wave modelling is that a considerable part of errors in the wave field is caused by errors in the wind field. It is by no means claimed that there are no errors in the wave models themselves, far from it, but the quality of the wind field is dominating the quality of the wave analysis and forecast. This is easily un-

derstood referring to the similarity analyses of the previous section. There we found that for old wind sea the dimensionless wave variance becomes constant. In terms of the significant wave height we find

$$H_s \sim U_{10}^2$$

and therefore a 10% error in wind speed gives a 20% error in wave height. This sensitive dependence on wind speed may be used in a positive sense. If one has reliable wave data, and if the wave model gives reasonable results, then observed wave heights could be utilised to provide useful information on the state of the atmosphere.

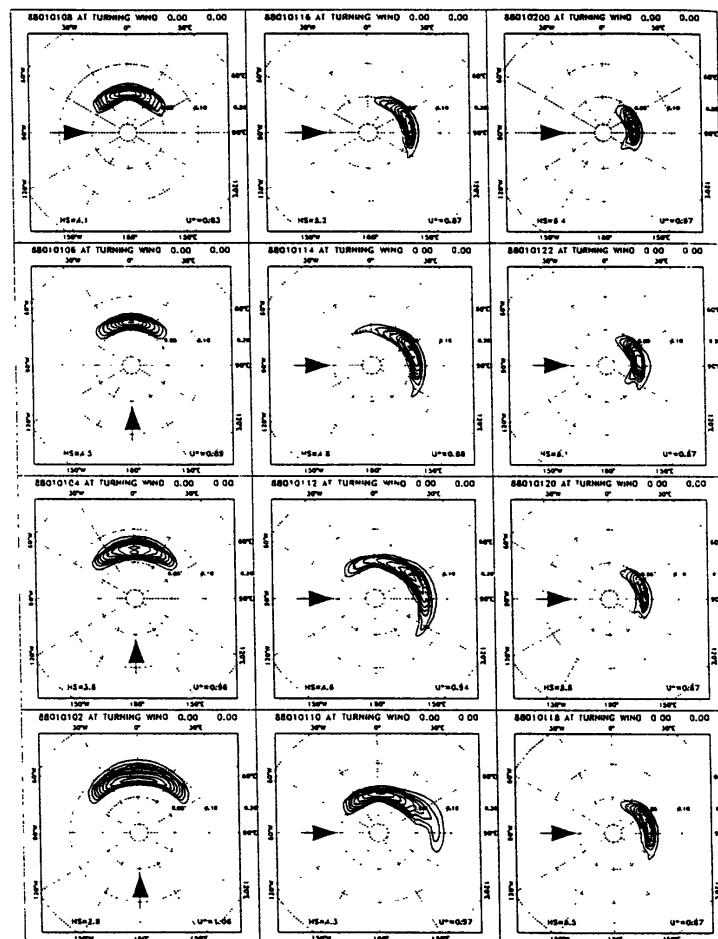


Figure 21. Evolution of two-dimensional spectrum for a turning wind field. Wind is turned after 6 h by 90°.

However, assuming that we have reliable wave data, this all relies on the quality of the wave model. Although the discussion in the previous section may have increased the confidence in the performance of the wave model, it is good to have another example, now from real life. The case in question occurred during the Surface Wave Dynamics Experiment (SWADE). This was an extensive experiment carried out from October 1990 until March 1991 off the east coast of the United States. The primary objectives were to understand the dynamics of the evolution of the surface wave field and to determine the effect of waves on the air/sea transfer of momentum. In order to achieve these objectives, concerted efforts were made to measure the surface meteorology with sufficient accuracy and spatial coverage so that the surface wind field was known sufficiently accurately. In addition, a dense array of wave buoys was employed.

The main event occurred on 26 October 1990 with extreme wave heights of 8 m. This case is shown in [Fig. 22](#). The reason why I show this case is the following. Dotted lines show the wind speeds according to the then operational ECMWF model and, in the plots for wave height, the dotted line refers to the WAM model as driven by the ECMWF winds. It is clear that, compared with the observed winds and waves, the modelled ECMWF winds and WAM wave heights are too low, especially during the extreme events. On the other hand, the full lines give a much better agreement with observations. These winds were obtained by Ocean Weather/Atmospheric Environment Service (OW/AES) and are the result of a man-machine mix procedure that takes maximum advantage of all the available tools and information: numerical modelling, the know-how of the experienced meteorologist and the measured sea state. The manual analysis makes use of all available pressure, temperature, ship and buoy data. Data are screened for inconsistencies and measured winds are adjusted for height. Anyway, in this way, high-quality wind fields were obtained and, as a result, the WAM model shows very good agreement when comparing modelled and observed wave height. The wave model is, therefore, a useful tool for quality control of the atmospheric state over the oceans.

Validation of wind and wave analysis using ERS-1 and buoy data

Fortunately, the quality of the ECMWF wind field is usually better than in the last example, although it should be emphasised that the wave results are usually the worst at the east coast of the USA.

The quality of wind and wave forecast is monitored daily by the analysts here at ECMWF. In addition, wind and wave quality is checked daily by comparing modelled results with altimeter data from ERS-1. An example is provided in [Figs. 23–24](#). Every month collocations of observed and modelled wave height and wind speed are collected and used to produce scatter plots displayed in [Figs. 25–26](#). It is emphasised that, regarding the wave height, we compare the six-hour first-guess wave height with altimeter wave height because nowadays in the wave analysis we use altimeter data to obtain an optimal analysis. Comparison with the six-hour first-guess is a fair comparison, since the satellite then probes a completely different part of the globe. Anyway, the comparison between altimeter and modelled data shows a very good agreement. The standard deviation of error for wind speed is below 2 m/s while that for wave height is about 40 cm. By comparison, it should be noted that during the Seasat period (September, 1978) the standard deviation of error for wave height was about 1 m ([Janssen *et al*, 1989](#)) thus considerable progress has been achieved over the years.

It must be pointed out in this context that altimeter data are not free of error. When compared with buoy data, the altimeter underestimates the wave height, especially in extreme cases. This may amount to an underestimation by as much as 10%. However, it is only fair to point out that buoys also have their problems under extreme conditions. Try to imagine how a buoy with a mast of 5 m height would behave in a 10 m wave field. In any event, it is of interest to compare wave model results with buoy data. A few examples, for March 1995, may be found in [Figs. 27–28](#). These examples show that, in general, the modelled wave heights underestimate the observed wave height, despite the reasonably good agreement between observed and modelled analysed winds. This may come as a surprise because the altimeter data comparison gave a somewhat different picture. The confusion is most likely caused by the fact that the observed buoy winds are assimilated in the ECMWF atmospheric model (for this reason there is good agreement in wind speed) but the observed winds have not been corrected for standard height. Since buoys observed the wind typically at a height of 4–5 m, this may result in a slowing down of the air flow by some 10–15%. This may explain the underprediction of wave height. On the other hand, one cannot fully exclude the possibility that the altimeter underestimates the wave height.

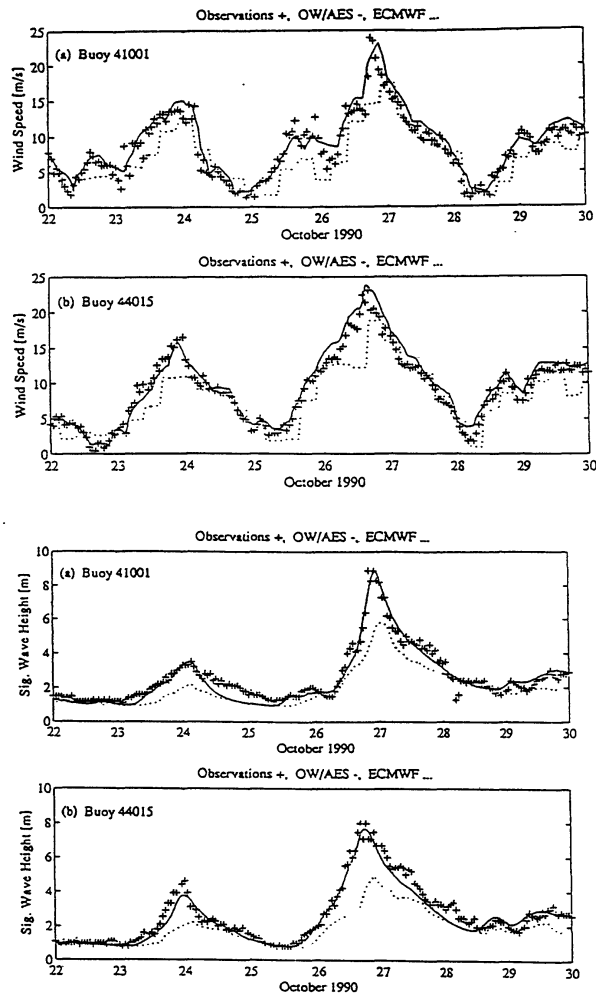


Figure 22. Comparison between the significant wave height recorded at the two positions and the corresponding values obtained using the ECMWF and OW/AES wind.

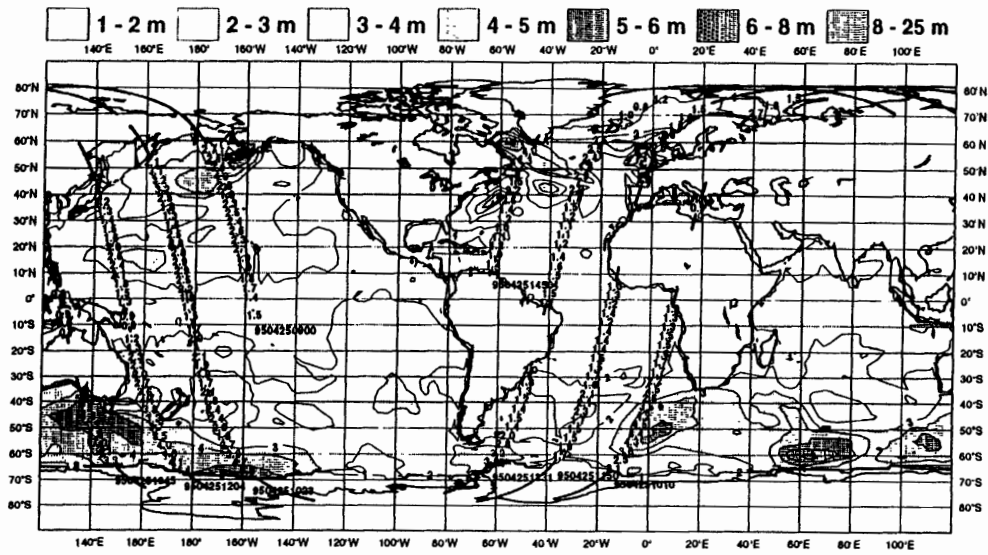


Figure 23. Collocation of altimeter and modelled wave height.

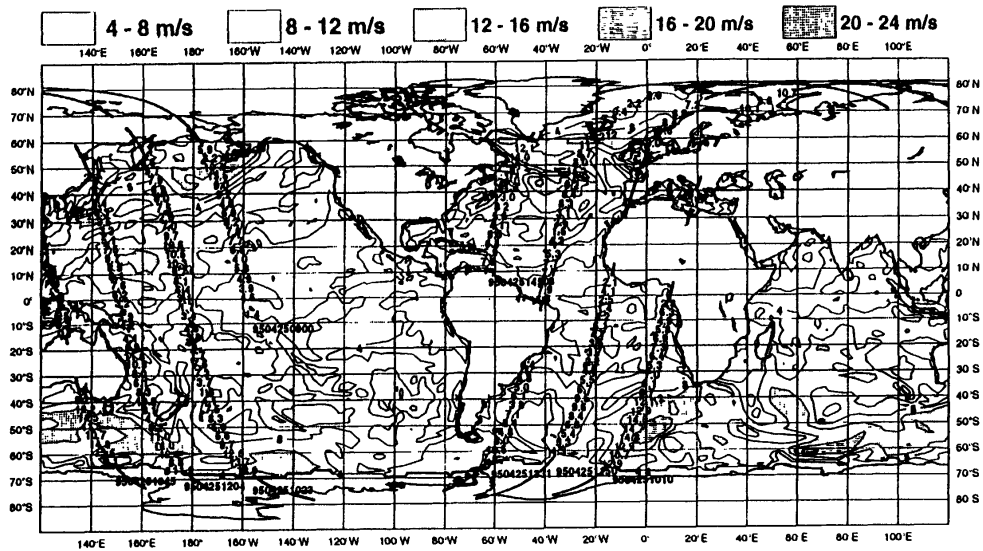


Figure 24. Collocation of altimeter and modelled wind speed.

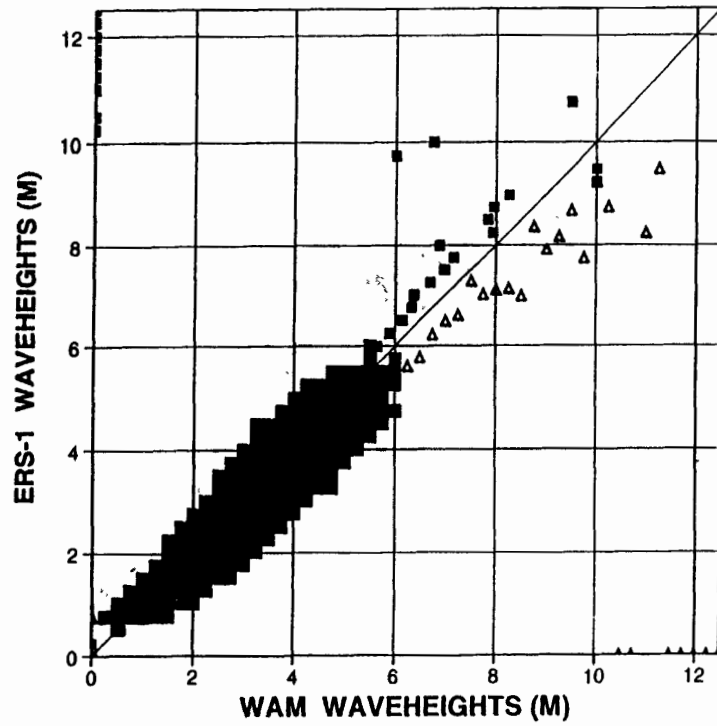


Figure 25. Scatter plot of altimeter versus modelled wave height.

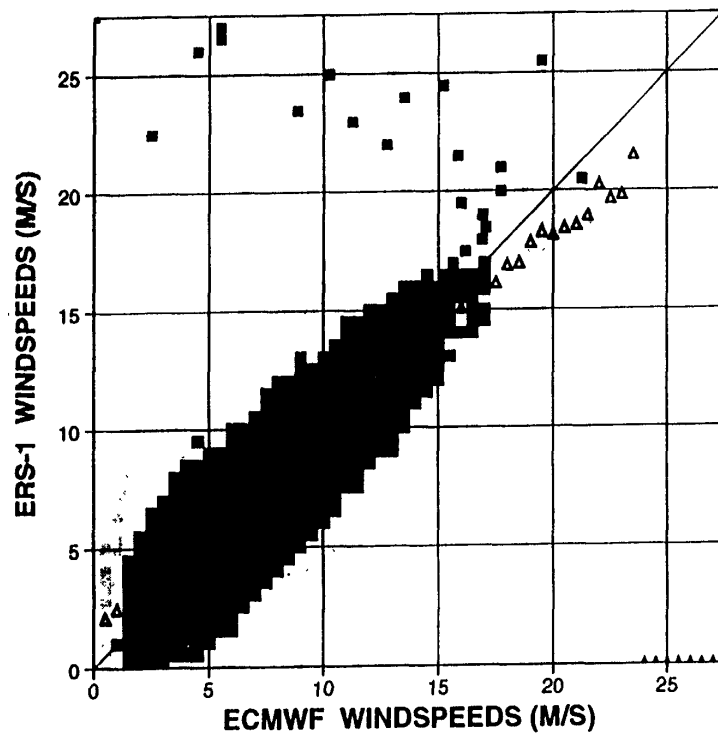


Figure 26. Scatter plot of altimeter versus modelled wind speeds.

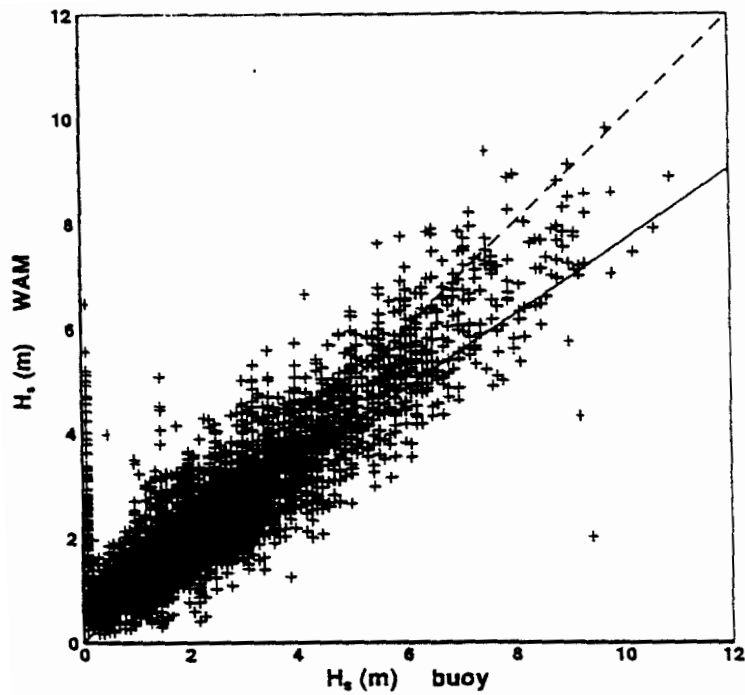


Figure 27. Comparison of European Centre ocean wave heights with buoy observations.

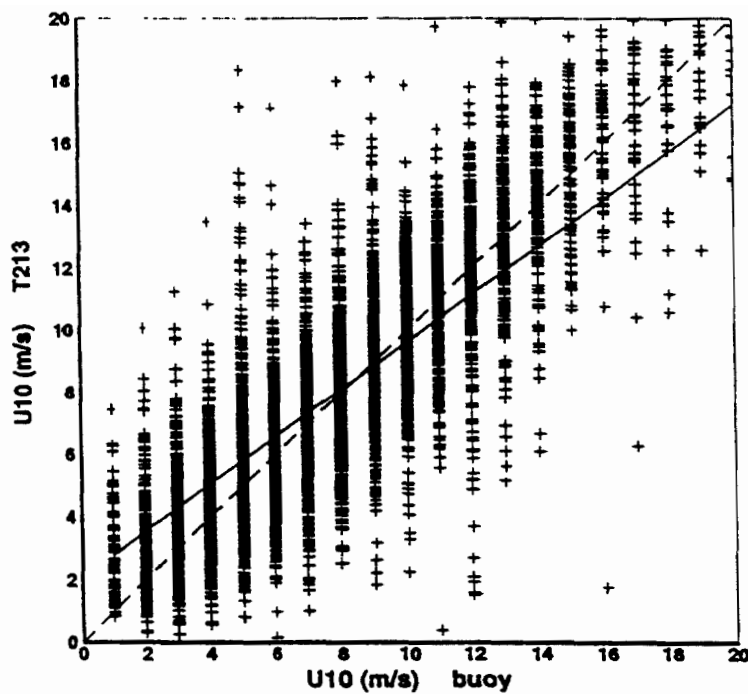


Figure 28. Comparison of European Centre surface winds with buoy observations.

Nevertheless, it should be evident that, when considering the standard deviation of error, there is better agreement with the altimeter data than with the buoy data. A probable reason that explains this discrepancy is related to the representativeness of the observation. In the case of the altimeter data we have an observation along the satellite track every 7 km. We obtain a superobservation from these data by averaging 30 observations. The superobserva-



tion thus obtained represents the state of the wave field over a line of about 200 km length and is therefore a quantity which may be compared with the modelled wave height which represents an average over a box of $1.5^\circ \times 1.5^\circ$. Buoy observations are less useful in this context because they usually refer to a 20 min average ($\sim 10 - 20$ km) and, therefore, represent scales which are not present in the wave model.

Quality of wave forecast

The quality of the forecast is usually judged by a comparison with the verifying analysis. This, of course, requires some confidence in the quality of the analysis. In the previous section we have seen that, compared with the altimeter data, the standard deviation of error is of the order of 50 cm and is, therefore, quite small.

In Figs. 29 –31 show forecast verification scores for the Northern Hemisphere, Tropics and the Southern Hemisphere. The left upper panel shows the mean error of forecast, the right upper panel shows the standard deviation of error of the forecast, the left lower panel shows the mean of the analysis, while the right lower panel gives the persistence error (persistence assumes that the state does not change in time and is given by the analysis at the time the forecast was started). These quantities are plotted as a function of forecast day, and we have taken the average over the three-month period from January until March 1995. Here, we concentrate on the standard deviation of error and, by comparing the error of the forecast with the one for persistence, we conclude that in the Northern Hemisphere, Tropics and Southern Hemisphere we have a useful forecast up to day 10, because the forecast error is always smaller than the persistence error. Nevertheless, it appears that the error growth is different in the storm tracks of the Southern and Northern Hemisphere (mainly wind waves!) than in the Tropics. In order to quantify this I have determined the relative rate of change of forecast error σ , defined as

$$\frac{1}{H_s} \frac{\partial \sigma}{\partial t}$$

where H_s is the average wave height over the area in question. Approximating the time derivative by the difference between day 3 and analysis error for the Northern and Southern Hemisphere, I get a relative increase of 0.08 per day, while for the Tropics I get 0.05 per day. The tropical area is, therefore, more predictable in this sense. A possible reason for the better predictability in the Tropics may be given by noting that the sea state in the tropics is dominated by swell that has been generated by winds from a few days before. These winds are of a better quality because they are from a shorter forecast range, or even from an analysis. This simply depends on the travel time of the swell from the generation area towards the area of interest. On the other hand, in the storm tracks the predictability of the waves depends, to a larger extent, on the predictability of the surface winds because the sea state is more dominated by wind sea.

Finally, it is also of interest to study the daily variations in forecast error and standard deviation of forecast error. I have displayed these in Fig. 32 for the Northern Hemisphere for the period July until September 1994. Note the start of a new season in the Northern Hemisphere in September!

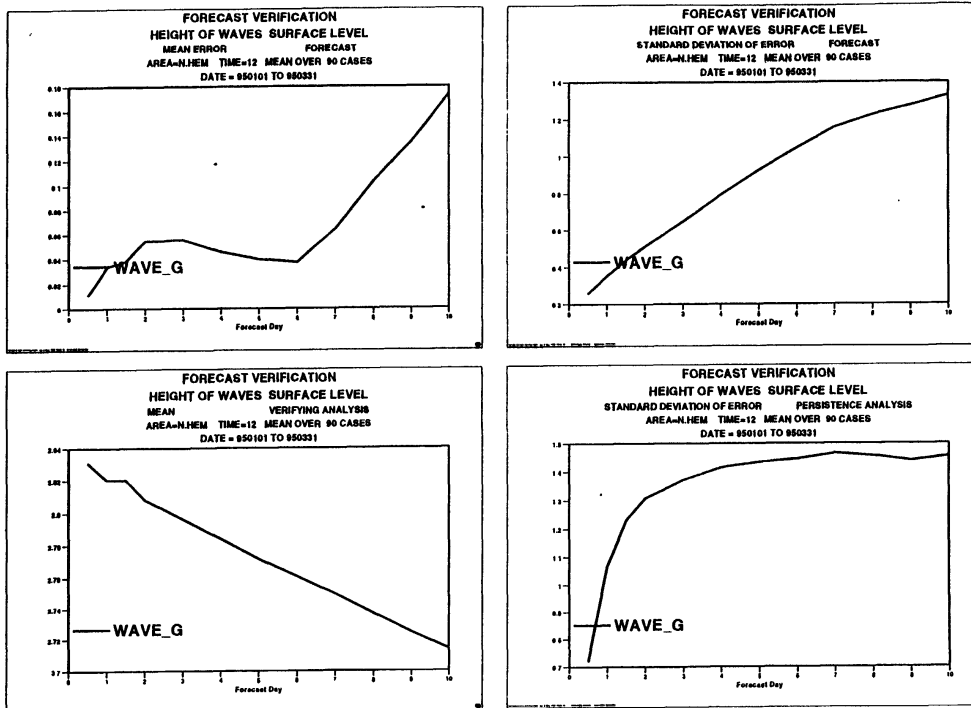


Figure 29. Forecast verification against analysis for Northern Hemisphere.

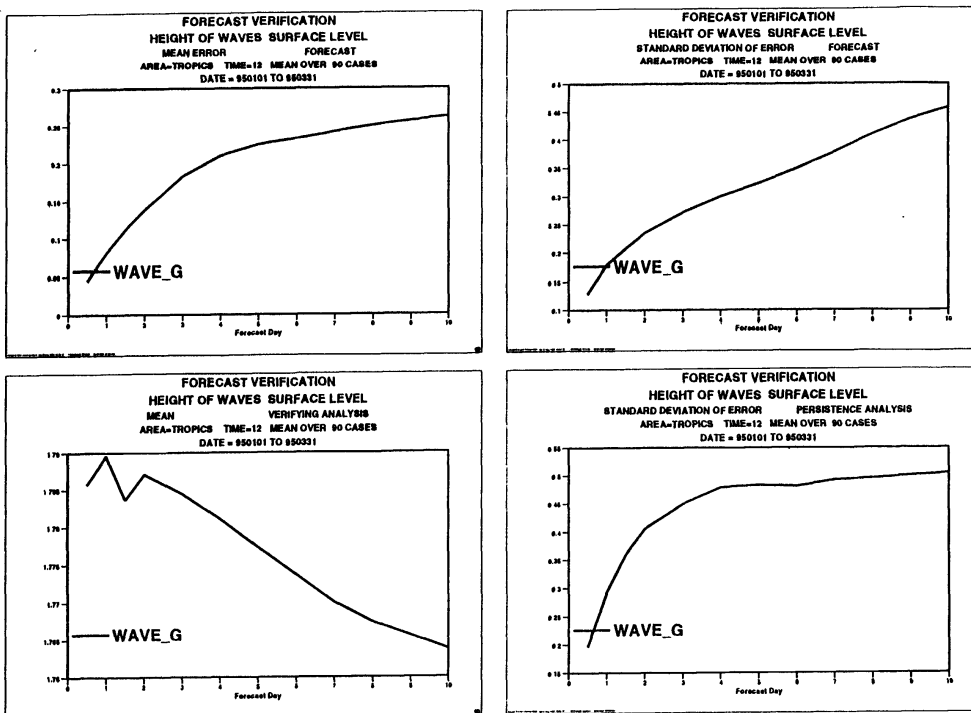


Figure 30. Same as Fig. 29 but now for Tropics.

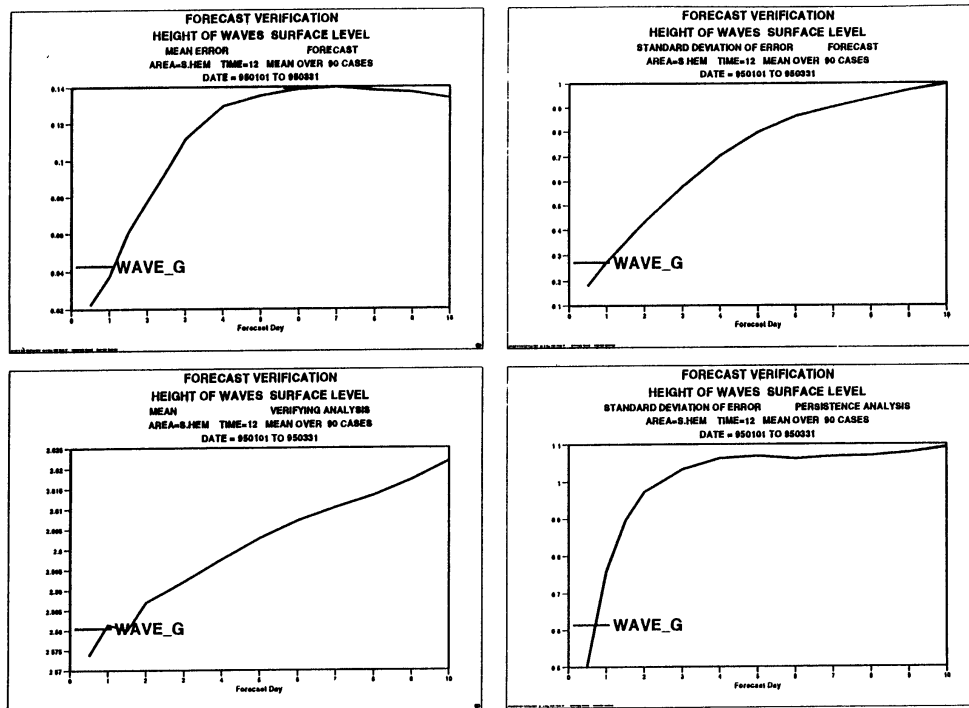


Figure 31. Same as Fig. 29 but now for Southern Hemisphere.

3. BENEFITS FOR ATMOSPHERIC MODELLING

In the final section I would briefly like to point out certain benefits of wave forecasting for atmospheric modelling. First of all, a wave model may be used as a diagnostic tool to search for problems in an atmospheric model. As an example we mention our analysis of the apparent over-activity of the atmospheric model during the forecast. Secondly, there are some suggestions that momentum and energy transfer from atmosphere to ocean is sea state dependent. In order to obtain a consistent momentum and energy balance, one has to couple wind and waves. Such a coupled wind–wave model gives an improved climate in the Northern Hemisphere.

3.1 Use as a diagnostic tool

Nowadays there are several examples known that show the benefits of ocean wave forecasting for atmospheric modelling. For example, by running the WAM model on surface stresses and surface winds from the ECMWF model, [Zambresky \(1986\)](#) found an inconsistency between the two. Typically, forcing with surface winds gave higher wave height in extreme events. This inconsistency was resolved by [Janssen et al. \(1992\)](#), who noted that the atmospheric model's time-split scheme, which treated physics and dynamics separately, had a time-step dependent equilibrium. An implicit treatment of both physics and dynamics removes this deficiency. When the semi-Lagrangian advection scheme is used, longer time steps are allowed and the use of the time-split scheme would have further enhanced the inconsistency between surface wind and stress. The new implicit integration scheme (applied to velocity, temperature and moisture) was therefore introduced with the semi-Lagrangian T213 version of the ECMWF model ([Ritchie et al., 1994](#)).

Another example is the apparent over-activity of the atmospheric model during the forecast. This is very evident from a plot of the mean forecast error in wave height as function of time. [Figs. 33–34](#) show this for the Northern

and Southern Hemisphere for the year 1994. The corresponding plots of the year 1993 showed a less severe problem. In this context it is also of interest to study the mean of the forecast wave field and the comparison with the analysed wave field. Figs. 35–39 therefore show the mean of analysis, day 1, day 3, day 5 and day 7 forecast for the month of May 1994. We point out that, in the Southern Hemisphere, there is an increase in wave height during the forecast reaching 1.5 m in certain small areas, while in the Tropics there is also a considerable increase over wide areas of about 0.5 m. Following the 2.5 m contour line during the forecast it seems that the increase in the Tropics is caused by too active a Southern Hemisphere storm track during the forecast.

Finally, we remark that this problem is fortunately less severe with subsequent model changes introduced on and after 4 April 1995.

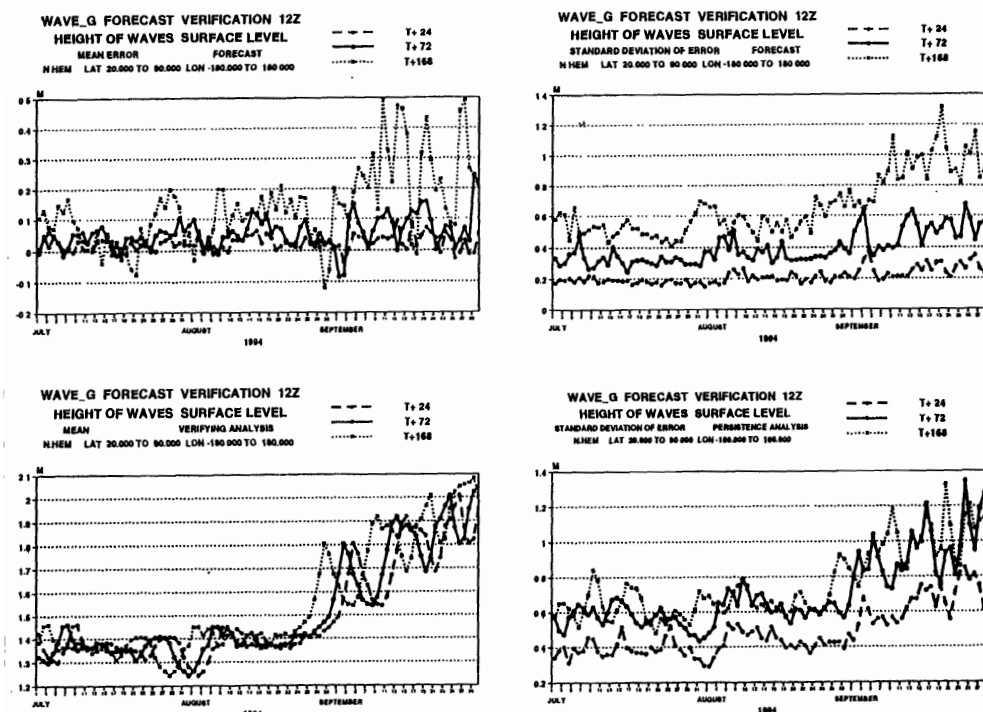


Figure 32. Daily error of forecast for days 1, 3 and 7. Period is July-September 1994. Area is Northern Hemisphere.

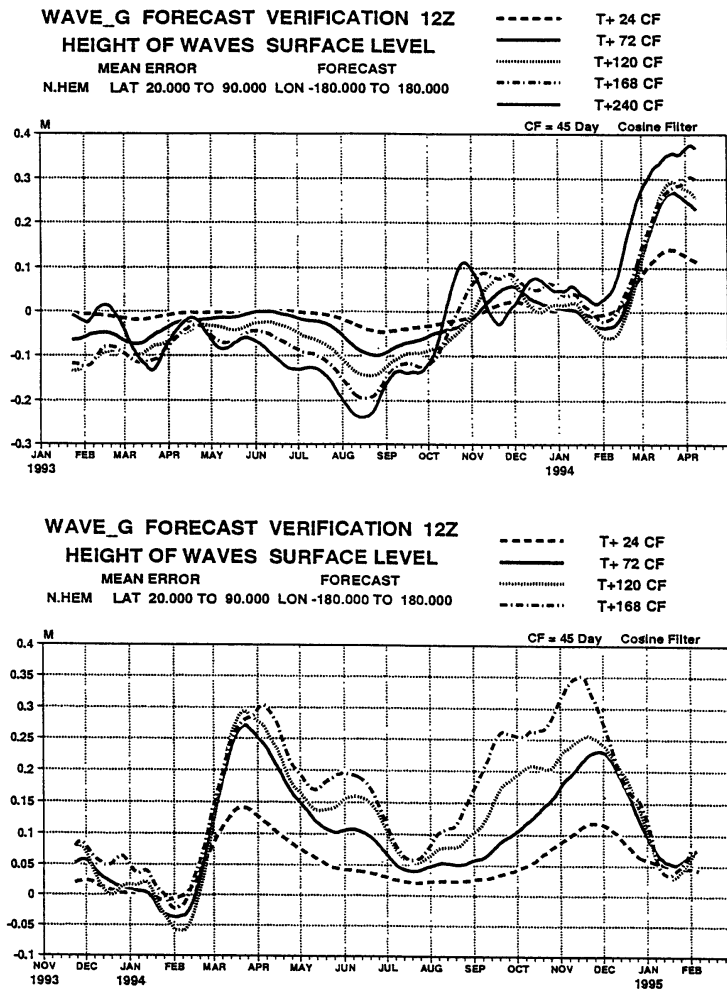


Figure 33. Mean forecast error for 1993 and 1994 in Northern Hemisphere.

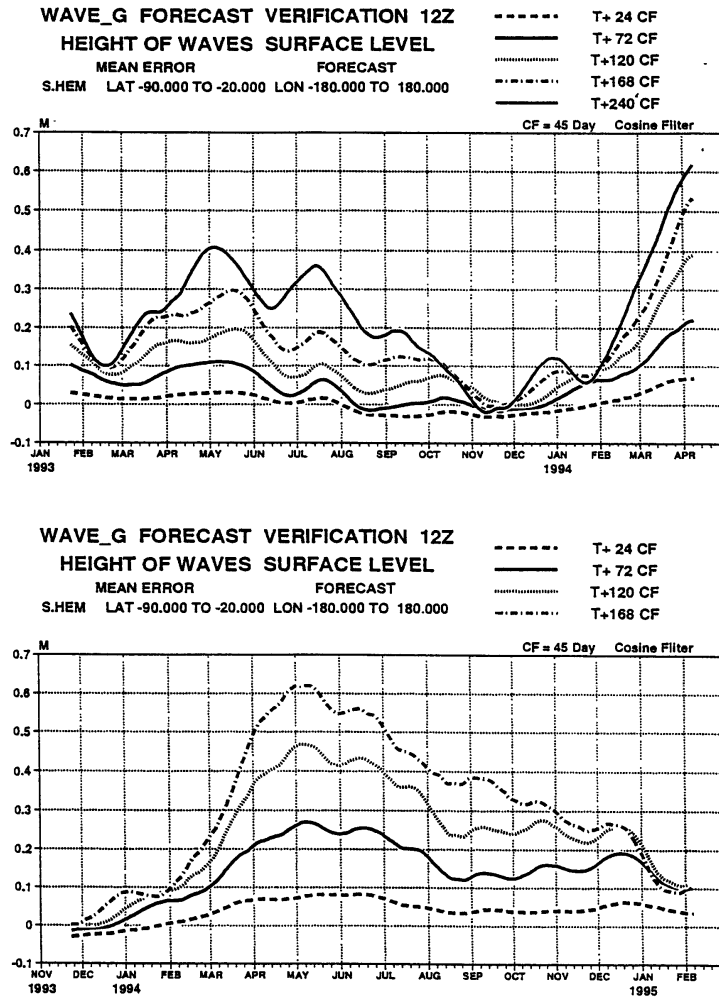


Figure 34. Mean forecast error for 1993 and 1994 in Southern Hemisphere

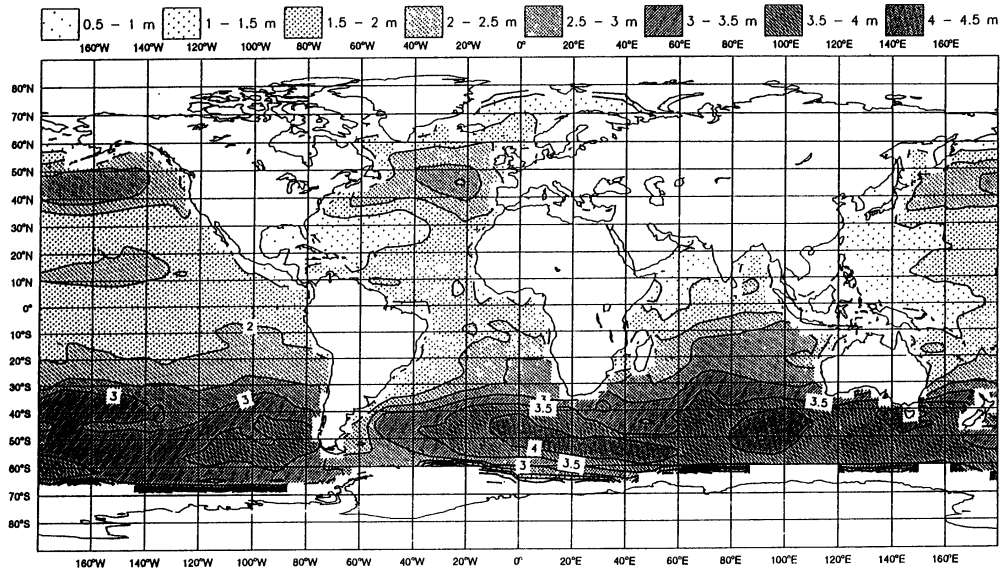


Figure 35. Monthly mean of analysis.

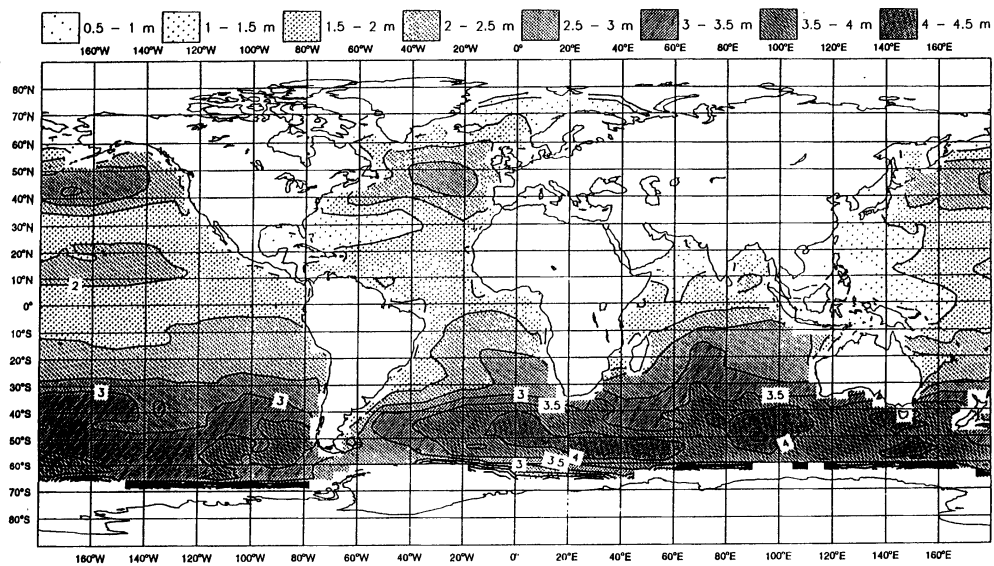


Figure 36. Monthly mean of day 1 forecast.

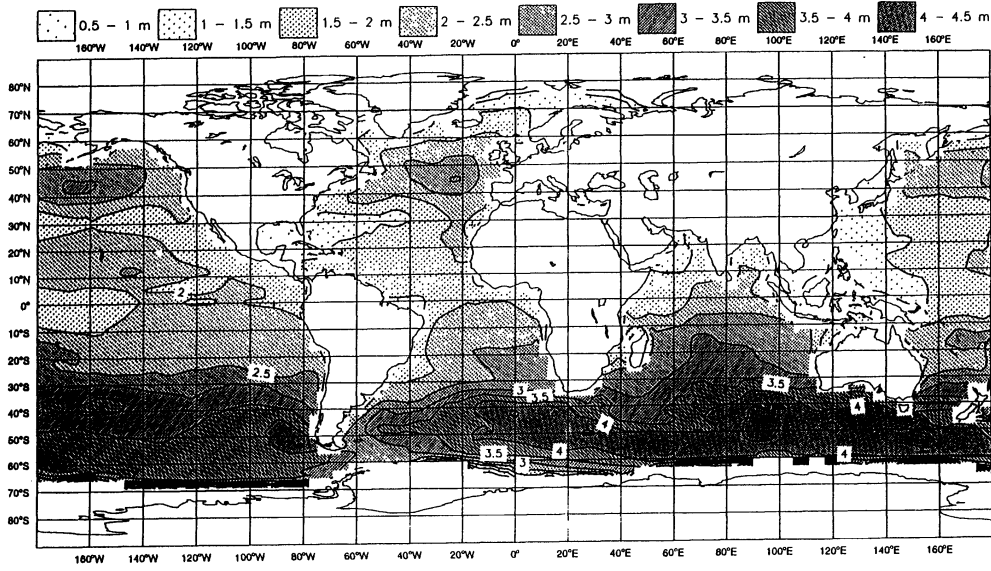


Figure 37. Monthly mean of day 3 forecast.

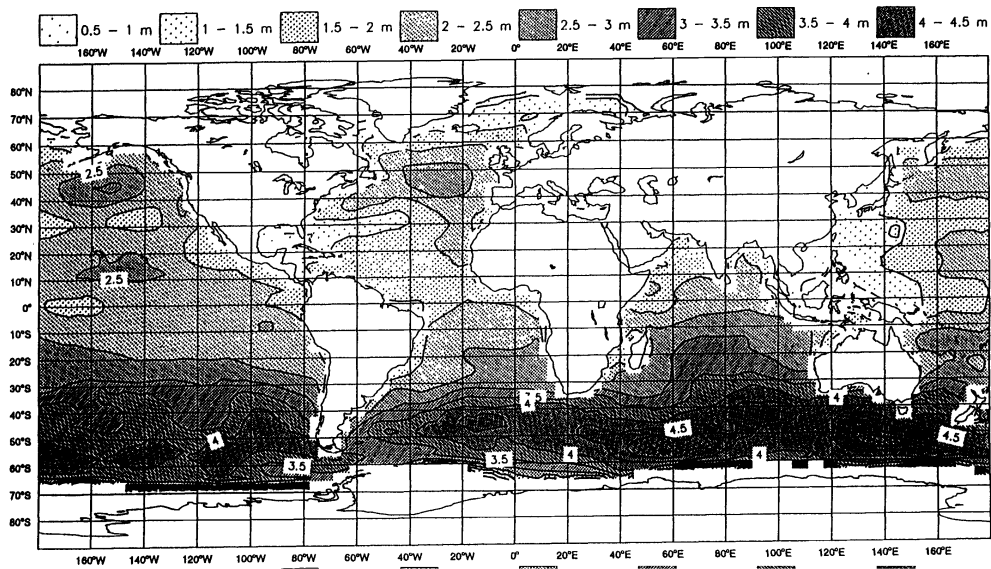


Figure 38. Monthly mean of day 5 forecast.

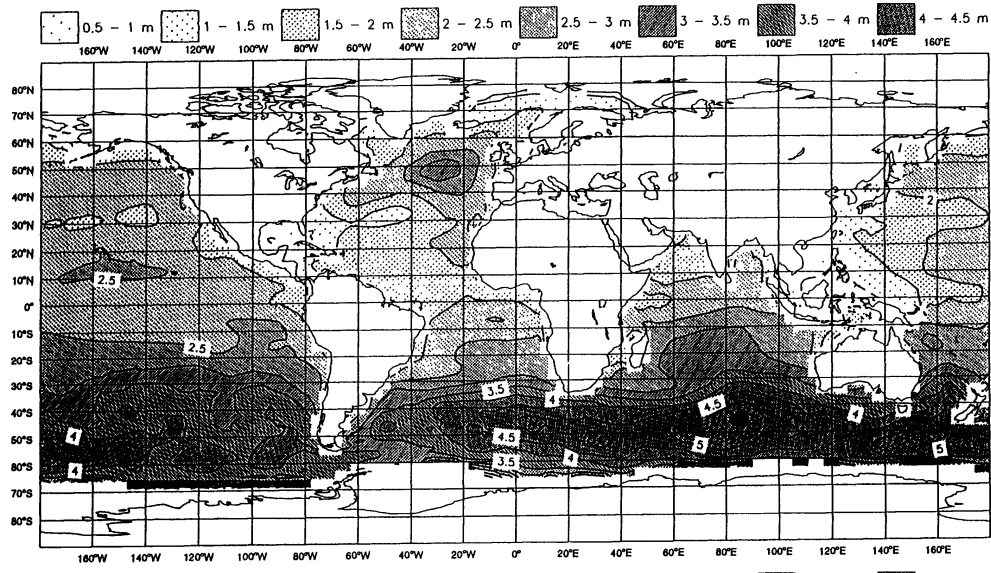


Figure 39. Monthly mean of day 7 forecast.

3.2 Coupled wind-wave modelling

We have already pointed out, on several occasions, that ocean waves may play a role in the momentum and energy transfer at the ocean surface. We have seen that young wind sea, which has steeper waves, will result in an enhancement of the drag coefficient by some 50%. The question now is to what extent this may have consequences for the large-scale atmospheric circulation.

In order to investigate this, Pedro Viterbo and I developed a coupled atmosphere, ocean-wave model (Janssen and Viterbo, 1995). In essence, the atmospheric model runs for one time step, then the ocean wave model is run next for one time step forced by the winds provided by the atmospheric model. Because one has explicit knowledge of the wind input term of the wave model, one may determine the wave-induced stress τ_w . This then gives information on the amount of slowing down of the air flow. We parametrized this slowing down by allowing the Charnock parameter to be a function of the wave-induced stress. We took (for more details on this cf Komen *et al.*, 1994) as Charnock parameter

$$\alpha = \beta \left(1 - \frac{\tau_w}{\tau} \right)^{-1/2}, \quad \beta = 0.01$$

and a considerable enhancement of the Charnock parameter is found when $\tau_w \cong \tau$. Note that, in a "steady" state, we always have $\tau_w < \tau$. The final step is then that the Charnock parameter is passed on to the atmospheric model which then performs a run with the updated α for one time step and so on.

Before I briefly discuss our results with climate runs it is instructive to study the impact of sea-state dependent momentum transfer on a single depression. This study was performed by Doyle (1994) who performed a sensitivity experiment by studying the evolution of a single depression with and without a sea state dependent Charnock parameter (called coupled and control). His results are displayed in Figs. 40–41 and they show that the relatively young wind sea will result in a rougher surface which apparently fills up the pressure low by about 6 mb on a timescale of 2.5 days. We remark that these results were obtained with a mesoscale model with horizontal resolution of 30 km.

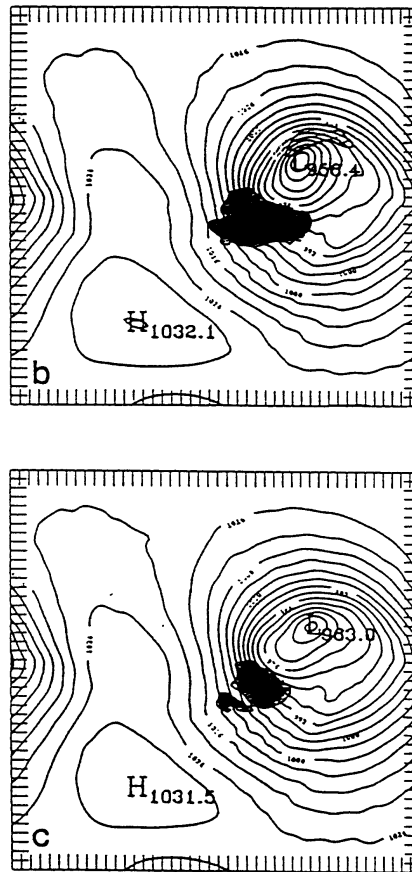


Figure 40. Simulated sea-level pressure for b) control and c) coupled simulations for the 60th time. The isopleth interval is 4 mb. Regions of lowest model layer wind speed in excess of 25 m/s are denoted by shading. Tick marks are plotted along the borders every third grid point or 90 km. (From Doyle, 1994, with permission.)

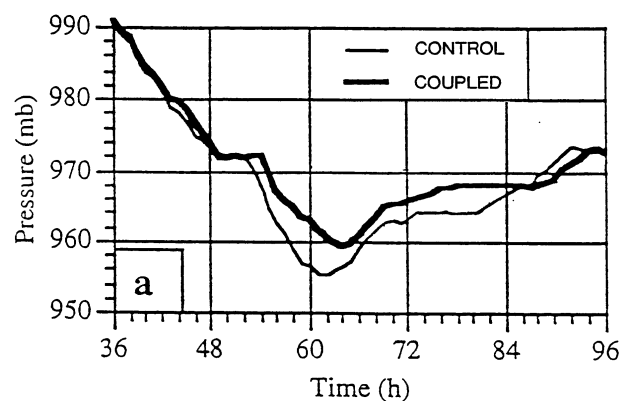


Figure 41. The corresponding central pressure trace of the cyclone.

Finally, I would like to present results Viterbo and myself obtained from extended-range runs. We performed 15 runs of 120 days long with the T63 version of the coupled model and we compared the mean over the last 90 days with results from the model in uncoupled mode (Charnock parameter $\alpha = 0.0185$). We took the winter season of 1990.

Fig. 42 shows the impact of waves on the atmospheric circulation in the Northern Hemisphere and the comparison with the analysed climate. We note a considerable improvement in 500 mb height field over Europe and Siberia in the coupled runs when comparing with the analysis.

A large-scale impact of waves on the atmospheric circulation is also noted in the Southern Hemisphere. There is, however, no improvement when results are compared with the analysis. In this context it should be pointed out that the Southern Hemisphere analysis is biased to a large extent towards the first-guess of the atmospheric model because of the lack of data. Therefore, the Southern Hemisphere analysis is more likely to resemble the climate simulation of the uncoupled model.

We close by remarking that we are still at the beginning of understanding the coupled ocean-wave/atmosphere model. It is expected, however, that ocean waves will play a role in future simulations of the earth climate by means of coupled atmosphere, ocean-circulation models. For one thing, waves have impact in the storm areas but, more importantly perhaps, ocean waves also affect the stress and wind field in the Tropics to a considerable extent. This is shown in the very last figure Fig. 43 where we have plotted the difference in wind field between coupled and control during the summer of 1989. As is evident, there are considerable differences in the monsoon area and in the warm pool area east of Indonesia. This will affect the temperature distribution of the ocean which, in its turn ..., etc.

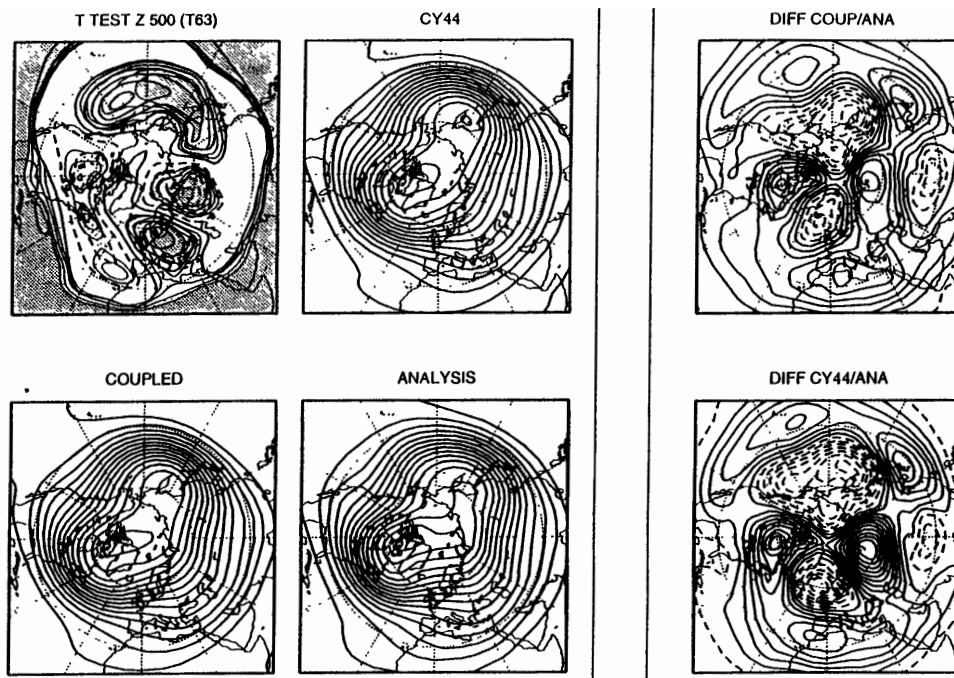


Figure 42. Comparison of coupled and control 500 mb fields with analysis period winter 1990.

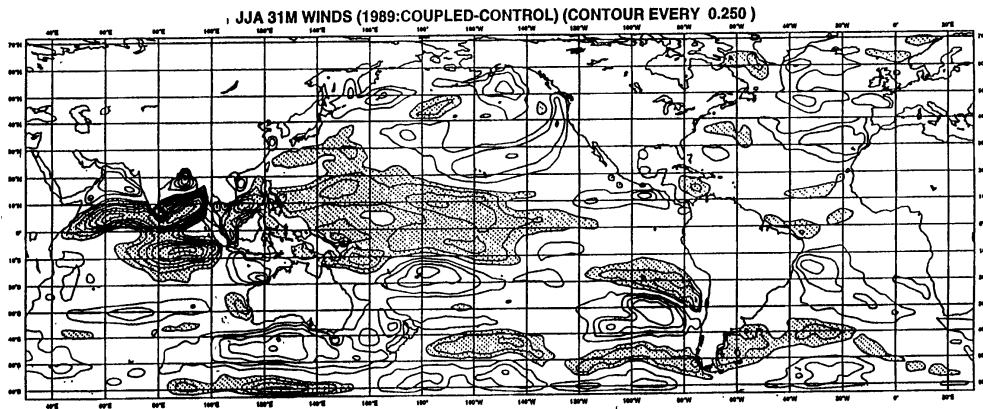


Figure 43. Difference in surface wind for summer 1989.

REFERENCES

- Broer, L J F, 1974: On the Hamiltonian theory of surface waves. *Appl Sci Res*, 30, 430-446.
- Brooke Benjamin, T and J E Feir, 1967: The disintegration of wave trains on deep water. *J Fluid Mech*, 27, 417-430.
- Charnock, H, 1955: Wind stress on a water surface. *Q J Royal Meteorol Soc*, 81, 639-640.
- Davidson, R C, 1972: *Methods in non-linear plasma theory*, Academic Press.
- Doyle, J D, 1994: Air-sea interaction during marine cyclogenesis. *Proc of the Life Cycles of Extratropical Cyclones*, Bergen.
- Drazin, P G and W H Reid, 1981: *Hydrodynamic stability*. Cambridge University Press, Cambridge, 525 pp.
- Hasselmann, K, 1962: On the non-linear energy transfer in a gravity-wave spectrum, part 1: general theory. *J Fluid Mech*, 12, 481.
- Janssen, P A E M, P Lionello, M Reistad and A Hollingsworth, 1989: Hindcasts and data assimilation studies with the WAM model during the Seasat period. *J Geophys Res*, C94, 973-993.
- Janssen, P A E M, A C M Beljaars, A Simmons and P Viterbo, 1992: On the determination of surface stresses in an atmospheric model. *Monthly Weather Review*, 120, 2977-2985.
- Janssen, P A E M and P Viterbo, 1995: Ocean waves and the atmospheric climate, submitted.
- JONSWAP: K Hasselmann et al, 1973: Measurements of wind-wave growth and swell decay during the Joint North Sea Wave Project (JONSWAP), *Dtsch Hydrogr Z Suppl A* 8(12), 95 p.
- Kitaigorodskii, S A, 1962: Application of the theory of similarity to the analysis of wind-generated water waves as a stochastic process, *Bull Acad Sci USSR Geophys*, Ser No. 1, 73 p.
- Komen, G J, L Cavaleri, M Donelan, K Hasselmann, S Hasselmann and P A E M Janssen, 1994: *Dynamics and modelling of ocean waves*, Cambridge University Press.
- Luke, J C, 1967: A variational principle for a fluid with a free surface. *J Fluid Mech*, 27, 395-397.
- Lighthill, M J, 1965: Contributions to the theory of waves on non-linear dispersive systems. *J Inst Math Appl*, 1,



269-306.

[Miles, J W](#), 1957: On the generation of surface waves by shear flows. *J Fluid Mech*, 3, 185-204.

[Miles, J W](#), 1977: On Hamilton's principle for surface waves. *J Fluid Mech*, 83, 153.

[Phillips, O H](#), 1960: The dynamics of unsteady gravity waves of finite amplitude, part 1. *J Fluid Mech*, 4, 426-434.

[Phillips, O M](#), 1977: *The dynamics of the upper Ocean*, 2nd edn, Cambridge University Press.

[Plant, W J](#) and [J W Wright](#), 1977: Growth and equilibrium of short gravity waves in a wind-wave tank. *J Fluid Mech*, 82, 767-793.

[Ritchie, H](#), [C Temperton](#), [A Simmons](#), [M Hortal](#), [T Davies](#), [D Dent](#) and [M Hamrud](#), 1995: Implementation of the semi-Lagrangian method in a high-resolution version of the ECMWF forecast model. *Monthly Weather Review*, 123, 489-514.

[Snodgrass, F E](#), [G W Groves](#), [K Hasselmann](#), [G R Miller](#), [W H Munk](#) and [W M Powers](#), 1966: Propagation of ocean swell across the Pacific. *Philos Trans Roy Soc London*, A249, 431.

[Snyder, R L](#), [F W Dobson](#), [J A Elliott](#) and [R B Long](#), 1981: Array measurements of atmospheric pressure fluctuations above surface gravity waves. *J Fluid Mech*, 102, 1-59.

[Stokes, G G](#), 1847: On the theory of oscillatory waves. *Trans Camb Phil Soc*, 8, 441-455.

[Whitham, G B](#), 1974: *Linear and non-linear waves*, Wiley.

[Yuen, H C](#) and [B M Lake](#), 1982: Nonlinear dynamics of deep water gravity waves. *Adv Appl Mech*, 22, 67-229.

[Zakharov, V E](#), 1968: Stability of periodic waves of finite amplitude on the surface of a deep fluid. *J Appl Mech Techn Phys*, 9, 190-194.

[Zambresky, L](#), 1986: The WAMS project, study III. Unpublished Report 116 p [Available from KNMI PO Box 201, 3730 AE de Bilt, The Netherlands].